Safety Analysis Opportunities Using Pavement Surface Characterization Based on 3D Laser Mapping

U.S. Department of Transportation
Federal Highway Administration

Safe Roads for a Safer Future
Investment in roadway safety saves lives

http://safety.fhwa.dot.gov

Notice

This document is disseminated under the sponsorship of the U.S. Department of Transportation in the interest of information exchange. The U.S. Government assumes no liability for the use of the information contained in this document. This report does not constitute a standard, specification, or regulation. The U.S. Government does not endorse products or manufacturers. Trademarks or manufacturers' names appear in this report only because they are considered essential to the objective of the document.

Quality Assurance Statement

The Federal Highway Administration (FHWA) provides high-quality information to serve Government, industry, and the public in a manner that promotes public understanding. Standards and policies are used to ensure and maximize the quality, objectivity, utility, and integrity of its information. FHWA periodically reviews quality issues and adjusts its programs and processes to ensure continuous quality improvement.

The U.S. Government does not endorse products, manufacturers, or any specific methodology created by any one entity. Trademarks, manufacturers' names, and developers of specific methodologies appear in this report for informational exchange only and because they are considered essential to the objective of the document.

Technical Report Documentation Page

1. Report No. FHWA-SA-17-046	**2. Government Accession No.**	**3. Recipient's Catalog No.**
4. Title and Subtitle Safety Analysis Opportunities Using Pavement Surface Characterization Based on 3D Laser Imaging		**5. Report Date** September 2017 **6. Performing Organization Code** HSA
7. Author(s) **Kelvin C. P. Wang, Qiang "Joshua" Li**		**8. Performing Organization Report No.**
9. Performing Organization Name and Address School of Civil and Environmental Engineering Oklahoma State University (OSU) Stillwater OK 74078		**10. Work Unit No. (TRAIS)** HSST **11. Contract or Grant No.** RFQ 50-53-14064
12. Sponsoring Agency Name and Address Federal Highway Administration - Office of Safety U.S. Department of Transportation 1200 New Jersey Avenue, SE Washington, DC0590		**13. Type of Report and Period Covered** Safety Analysis Report March 2014 to March 2016 **14. Sponsoring Agency Code** HSA

15. Supplementary Notes
Joseph Cheung (joseph.cheung@dot.gov), Office of safety served as the Technical Manager for FHWA. The following FHWA staff members contributed as technical working group members, reviewers and/or provided input or feedback to the project at various stages: Frank Julian, Jim Sherwood, Andy Mergenmeier, Mike Moravec (retired), Mark Swanlund.

16. Abstract

Pavement surface properties play critical roles in maintaining proper interaction between tire and pavement, and necessary drainage runoff for both pavement and safety management. Currently, data collection and analysis of pavement surface properties, such as texture and profiling, have primarily relied on single line of measurements using multiple vehicles to obtain a comprehensive evaluation of pavement surface properties. This project serves to demonstrate the use of state-of-the-art 3-D Ultra Laser imaging data collection methodology with integrated data platform, higher data resolution, full-width pavement coverage, less interruption to traffic, and more robust software solutions will result in a more efficient and cost-effective data collection process and may potentially lead to new measurement standards. Specifically, three applications based on 3D Ultra have been investigated in this study for various aspects of pavement surface safety analysis:

- Effectiveness and performance of High Friction Surface Treatment (HFST) at a national scale,
- Investigation of geometric texture indicators for pavement safety with 1mm 3D data,
- Evaluation of pavement surface hydroplaning with 1mm 3D data.

17. Key Words pavement safety, pavement texture, High Friction surface Treatments, pavement friction, surface characteristics, 3D Laser Imaging, hydroplaning	**18. Distribution Statement** No restrictions.

19. Security Classif. (of this report)	**20. Security Classif. (of this page)**	**21. No. of Pages**	**22. Price**
Unclassified	Unclassified	63	

Form DOT F 1700.7 (8-72) **Reproduction of completed page authorized**

SI* (MODERN METRIC) CONVERSION FACTORS

APPROXIMATE CONVERSIONS TO SI UNITS				
SYMBOL	**WHEN YOU KNOW**	**MULTIPLY BY**	**TO FIND**	**SYMBOL**
		LENGTH		
in	inches	25.4	millimeters	mm
ft	feet	0.305	meters	m
yd	yards	0.914	meters	m
mi	miles	1.61	kilometers	km
		AREA		
in^2	square inches	645.2	square millimeters	mm^2
ft^2	square feet	0.093	square meters	m^2
yd^2	square yard	0.836	square meters	m^2
ac	acres	0.405	hectares	ha
mi^2	square miles	2.59	square kilometers	km^2
		VOLUME		
fl oz	fluid ounces	29.57	milliliters	mL
gal	gallons	3.785	liters	L
ft^3	cubic feet	0.028	cubic meters	m^3
yd^3	cubic yards	0.765	cubic meters	m^3
	NOTE: volumes greater than 1000 L shall be shown in m^3			
		MASS		
oz	ounces	28.35	grams	g
lb	pounds	0.454	kilograms	kg
T	short tons (2000 lb)	0.907	megagrams (or "metric ton")	Mg (or "t")
		TEMPERATURE (exact degrees)		
°F	Fahrenheit	5 (F-32)/9	Celsius	°C
		ILLUMINATION		
fc	foot-candles	10.76	lux	lx
fl	foot-Lamberts	3.426	$candela/m^2$	cd/m^2
		FORCE and PRESSURE or STRESS		
lbf	poundforce	4.45	newtons	N
lbf/in^2	poundforce per square inch	6.89	kilopascals	kPa

APPROXIMATE CONVERSIONS FROM SI UNITS				
SYMBOL	**WHEN YOU KNOW**	**MULTIPLY BY**	**TO FIND**	**SYMBOL**
		LENGTH		
mm	millimeters	0.039	inches	in
m	meters	3.28	feet	ft
m	meters	1.09	yards	yd
km	kilometers	0.621	miles	mi
		AREA		
mm^2	square millimeters	0.0016	square inches	in^2
m^2	square meters	10.764	square feet	ft^2
m^2	square meters	1.195	square yards	yd^2
ha	hectares	2.47	acres	ac
km^2	square kilometers	0.386	square miles	mi^2
		VOLUME		
mL	milliliters	0.034	fluid ounces	fl oz
L	liters	0.264	gallons	gal
m^3	cubic meters	35.314	cubic feet	ft^3
m^3	cubic meters	1.307	cubic yards	yd^3
		MASS		
g	grams	0.035	ounces	oz
kg	kilograms	2.202	pounds	lb
Mg (or "t")	megagrams (or "metric ton")	1.103	short tons (2000 lb)	T
		TEMPERATURE (exact degrees)		
°C	Celsius	1.8C+32	Fahrenheit	°F
		ILLUMINATION		
lx	lux	0.0929	foot-candles	fc
cd/m^2	$candela/m^2$	0.2919	foot-Lamberts	fl
		FORCE and PRESSURE or STRESS		
N	newtons	0.225	poundforce	lbf
kPa	kilopascals	0.145	poundforce per square inch	lbf/in^2

*SI is the symbol for the International System of Units. Appropriate rounding should be made to comply with Section 4 of ASTM E380.
(Revised March 2003)

TABLE OF CONTENTS

LIST OF FIGURES

LIST OF TABLES

1. INTRODUCTION

Pavement surface properties play critical roles in maintaining proper interaction between tire and pavement, and necessary drainage runoff for both pavement and safety management. Currently, data collection and analysis of pavement surface properties, such as texture and profiling, have primarily relied on single line of measurements. Frequently highway agencies have to use multiple vehicles to obtain a comprehensive evaluation of pavement surface properties. Further, despite of continuous improvements of sensing methodologies in the past decades, many of the instrumentations used today are still based on decades old technologies. Therefore implementing art-of-the-state data collection methodology with integrated data platform, higher data resolution, full-width pavement coverage, less interruption to traffic, and more robust software solutions will result in a more efficient and cost-effective data collection process and may potentially lead to new measurement standards.

This project is a response to the requisition number RFQ 50-53-14064 solicited by the Federal Highway Administration (FHWA). The 3D laser imaging technology, named as PaveVision3D Ultra (3D Ultra for short) developed by the WayLink Systems Corporation in collaboration with the Oklahoma State University (OSU), is used in this study for multiple safety and pavement evaluation purposes. 3D Ultra is designed on a single-pass and complete lane-coverage platform for data collection on roadways capable of operating at highway speeds up to 60mph (96.5 km/h) at 1mm resolution, and can collect data for automated pavement measurements for texture, smoothness, friction, and distresses with necessary software tools. Specifically, three applications based on 3D Ultra have been investigated in this study for various aspects of pavement surface safety analysis:

- **Effectiveness and performance of High Friction Surface Treatment (HFST) at a national scale**: Although HFST has been widely installed in recent years in many states, validation efforts considering various aggregate types and the bonding materials, installation ages, environmental conditions, and traffic volumes are not as comprehensive as desired. The use of high-speed data collection systems as demonstrated in this project may improve such validation efforts. . Utilizing 3D Ultra and FHWA's fixed-slip continuous friction tester, this study collects comprehensive pavement surface data at 21 HFST sites in 11 states at highway speeds. Measurements on HFST and untreated pavements are compared to determine the effectiveness of HFST. Multivariate analyses are conducted to investigate the impacts of various factors listed above on HFST friction performance. Through the use of 3D Ultra, friction models are developed to aid highway agencies in managing HFST.

- **Investigation of geometric texture indicators for pavement safety with 1mm 3D data**: Surface texture and friction are two primary characteristics for pavement safety evaluation. Understanding their relationship is critical to reduce potential traffic crashes especially in wet conditions. Currently Texture data obtained from existing systems are limited to either a small portion of the pavement surface or one single line of longitudinal profile, and the currently used texture indicators, such as Mean Profile Depth (*MPD*), and Mean Texture Depth (*MTD*) only reveal partial aspects of texture properties of interest.

With the 1mm 3D data collected from 3D Ultra, four types of texture indicators (amplitude, spacing, hybrid, and functional parameters) are calculated to represent various texture properties for pavement friction estimation. The relationships among those texture indicators and pavement friction are examined. The contributing texture parameters are identified for pavement friction prediction, and subsequently a multivariate regression pavement friction model is developed to aid the evaluation of pavement safety for project- and network- level pavement surveys.

- **Evaluation of pavement surface hydroplaning with 1mm 3D data**: During high intensity rainfall events, hydroplaning may occur and affect driver safety especially on sharp curves. Past studies indicate that an increase in hydroplaning risk occurs with an increase of the Water Film Depth (WFD), which is dependent on surface texture properties, flow path slope, flow path length, rainfall intensity, and pavement surface type. However, little research work has been conducted to investigate pavement surface drainage at network levels because the existing data acquisition systems are incapable of continuously measuring related data sets at high speeds. This application utilizes 1mm 3D texture data continuously collected by 3D Ultra, and roadway geometric data acquired with an Inertial Measurement Unit (IMU) system for the prediction and evaluation of pavement surface hydroplaning risk. Due to the fact that the presence of longitudinal and cross slopes would decrease the wheel load of vehicles perpendicular to the pavement surface and increase hydroplaning risk, two improved models based on the existing Gallaway and University of South Florida (USF) models are presented in this study. 1mm 3D pavement surface data is used to estimate texture information for the models in lieu of traditional spot-laser based texture measurement devices. A 4.35 km pavement section with five horizontal curves is selected to investigate and compare the speeds that lead to hydroplaning predicted from Gallaway and USF models, and the two improved models. Through this effort, pavement segments with potential hydroplaning risk are identified by comparing predicted speeds with posted speed limits.

2. DATA COLLECTION DEVICES

PaveVision3D Ultra

The PaveVision3D laser imaging system has evolved into a sophisticated system to conduct full lane data collection on roadways at highway speeds up to 60mph (96.5 km/h) at 1mm resolution. Figure 2.1 demonstrates the Digital Highway Data Vehicle (DHDV) equipped with PaveVision3D Ultra, which is able to acquire both 3D laser imaging intensity and range data from pavement surfaces through two separate sets of sensors. Recently, two 3D high resolution digital accelerometers have been installed on the system, capable of reporting compensated pavement surface profiles and generating roughness indexes. The collected data are saved by image frames with the dimension of 2,048 mm in length and 4,096 mm in width. In summary, the 1mm 3D pavement surface data can be used for:

- Comprehensive evaluation of surface distresses: automatic and interactive cracking detection and classification based on various cracking protocols;
- Profiling: transverse for rutting and longitudinal for roughness (Boeing Bump Index and International Roughness Index);
- Safety analysis: including macro-texture in term of mean profile depth (MPD) and mean texture depth (MTD), hydroplaning prediction, and grooving identification and evaluation;
- Roadway geometry: including horizontal curve, longitudinal grade and cross slope.

Figure 2.1. A PaveVision3D Ultra data collection vehicle used for the research

In addition, an Inertial Measurement Unit (IMU) with high accuracy has been integrated and synchronized into the 3D Ultra data vehicle for geometrical information capture. IMU is a self-contained sensor consisting of accelerometers, fiber-optic gyroscopes, and integrated GPS

antennas, whose data contain GPS coordinates, horizontal curve, longitudinal grade, and cross slope, and are utilized for hydroplaning speed prediction.

AMES 8300 High Speed Profiler

The AMES Model 8300 High Speed Profiler is designed to collect macro surface texture data along with standard profile data at highway speeds. Multiple texture indexes such as Mean Profile Depth (MPD) can be calculated from the testing data. This High Speed Profiler meets or exceeds the following requirements: ASTM E950 Class 1 profiler specifications, AASHTO PP 51-02 and Texas test method TEX 1001-S. The texture specifications of the Profiler include:

- Capable of collecting measurements at speeds between 25 and 65 mph
- Laser height sensor with a range of 180 mm and a resolution of 0.045 mm
- Horizontal distance measured with an optical encoder that has a resolution of 1.2 mm
- Pavement elevation sampling rate 62,500 samples per second
- Profile wavelength down to 0.5 mm

Figure 2.2 AMES 8300 high speed profiler used to collect Macro Surface Texture data and profile data

Dynatest 6875H Highway Friction Tester

The Federal Highway Administration (FHWA) is offering demonstrations of its Dynatest 6875H Highway Friction Tester (HFT) to state departments of transportation (DOTs). The HFT is a self-contained testing vehicle that maps friction at one-foot intervals continuously along a pavement section. Agencies can use friction data provided by the HFT for both network-level and project-level applications. Continuous friction testing can improve agencies' ability to measure friction through intersections and around curves, regardless of radius. As well as providing continuous friction testing, the HFT uses a fixed-slip test method to deliver a coefficient of friction more representative of conditions experienced by vehicles with modern anti-lock braking systems (ABS).

Figure 2.3 A Dynatest 6875H highway friction tester that maps friction continuously along a pavement section.
(From http://www.thetranstecgroup.com/fhwa-providing-friction-tester-demonstrations/)

3. EFFECTIVENESS AND PERFOMANCE OF HFST AT A NATIONAL SCALE

Introduction

High Friction Surface Treatments (HFST) were firstly applied in the United Kingdom in 1960s to maintain pavement skid resistance and reduce the fatalities and injuries from crashes that occur at or near horizontal curves [1]. Recently, the Surface Enhancements At Horizontal Curves program (SEaHC) administered under the FHWA Every Day Counts 2 program, HFST were installed at numerous horizontal curves throughout the U.S. due to higher friction demand of vehicles on curves than that on other pavement sections [2]. Through various HFST projects, the effectiveness of HFST in improving skid resistance and reducing crashes has been demonstrated [3, 4, 5, 6, 7, and 8]. Generally pavement friction and macro-texture are tested before and after HFST installation to quantify the changes in surface skid resistance. Pavement friction is measured primarily using the Dynamic Friction Tester and agency-owned locked-wheel skid testers, while macro-texture is measured using stationary or low speed devices such as the Circular Track Meter, ASTM E 965 "Sand Patch" Method, or RoboTex [4, 7]. Most of these devices require lane closure to perform the tests, and highway agencies must perform multiple data collection processes to gather different pavement surface characteristics. These limitations have constrained continuous evaluation and monitoring of the surface characteristics of installed HFST sites in the longer term after they are opened to traffic. In addition, based on our literature search, no study has been conducted to evaluate HFST performance at a national scale under various traffic conditions, environments, and HFST materials.

HFST Data Collection

HFST Sites

This 3D Ultra technology, which offers a single-pass and complete lane coverage platform at prevalent traffic speed, provides an ideal solution to evaluate the surface characteristics of HFST without interrupting traffic [9]. In addition, pavement friction data on HFST is collected using the FHWA fixed-slip continuous friction tester, which uses a standardized smooth-tread test tire to measure friction in terms of a unitless friction number, Mu.

The data collection effort described herein includes pavement friction and surface characteristics testing of 21 HFST sites in 10 states as instructed by FHWA. The locations of the HFST sites are shown in Figure 3.1. Considering both directions and total number of lanes, 41 data collection events were conducted, with each 3D data collection covering a full traffic lane. To determine the effectiveness of HFST in improving surface properties, surface characteristics including pavement cracking, rutting, macro-texture, friction, roadway geometry are measured for each HFST site. All data were collected beginning from 300 ft to 500 ft before the target HFST road section and 300 ft to 500 ft after each HFST section to capture these data for the existing pavement as well.

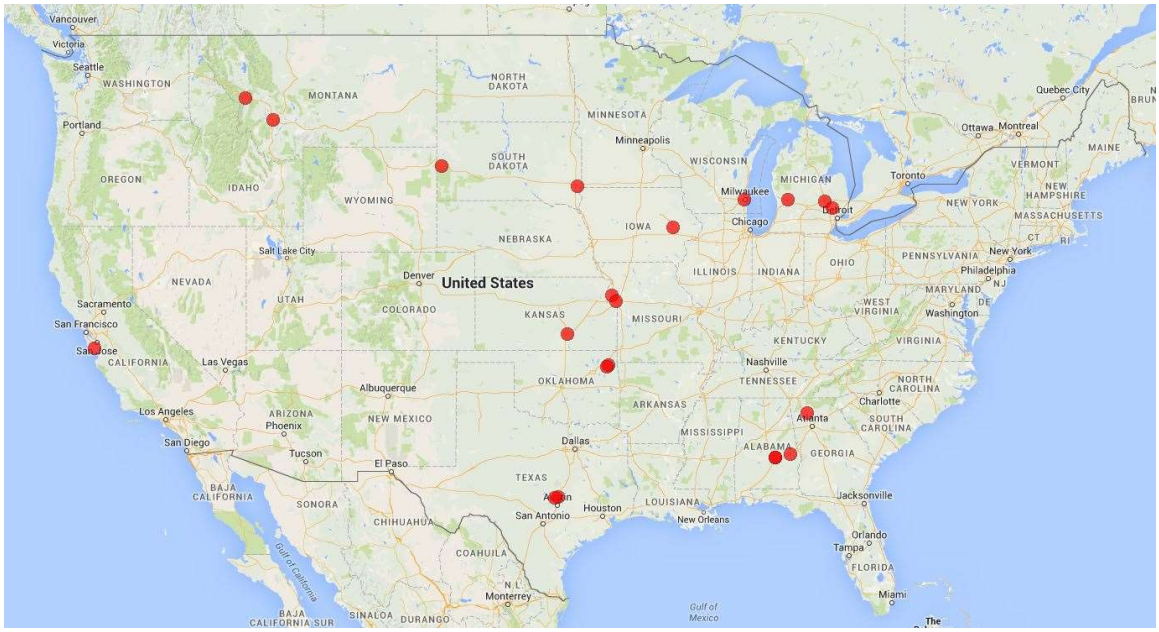

Figure 3.1. HFST sites

Pavement Surface Characterization

To determine the effectiveness of HFST in improving surface properties, the following surface characteristics were measured on-site at each HFST site before, within, and after each HFST section.

- Pavement cracking,
- Pavement rutting,
- Pavement macrotexture,
- Pavement friction,
- Roadway geometry.

Pavement Cracking

The AASHTO Designation PP67-10 outlines the procedures for quantifying cracking distresses at the network level [10]. The protocol is designed for fully automated surveys, while minimal human intervention is needed in the data processing. Three cracking types: transverse cracking, longitudinal cracking, and pattern cracking, are defined based on the orientation of the cracking spanning. The five traffic zones divide the entire lane coverage into wheel-path and non-wheel path areas. The total cracking length and average cracking width of each cracking type are reported for each zone. No cracking was observed on the pavement surface for majority of the HFST sites. Cracks were found only on two older HFST sites.

Pavement Rutting

Rutting is defined as the permanent traffic-associated deformation within pavement layers. The recent provisionally-approved AASHTO Designation PP69-10 [11] has been implemented into the 3D Ultra system for rutting characterization and cross slope measurements. Rutting in the left

and right wheelpaths are averaged into average rutting in inches for each image frame for each data collection. Rutting data are not calculated for rigid pavement sections, which are represented with zero rutting values.

Pavement Friction

Skid resistance is the ability of the pavement surface to prevent the loss of tire traction. The friction value from the HFST was reported every 1 ft over the length of the section tested in order to show any variations in friction. Example friction data plots are shown in Figure 3.2. Some sites show clear improvements of skid resistance (as shown in Figure 3.2a) and the differentiation of the HFST section from abutting pavement, while others don't show any trend (as shown in Figure 3.2b).

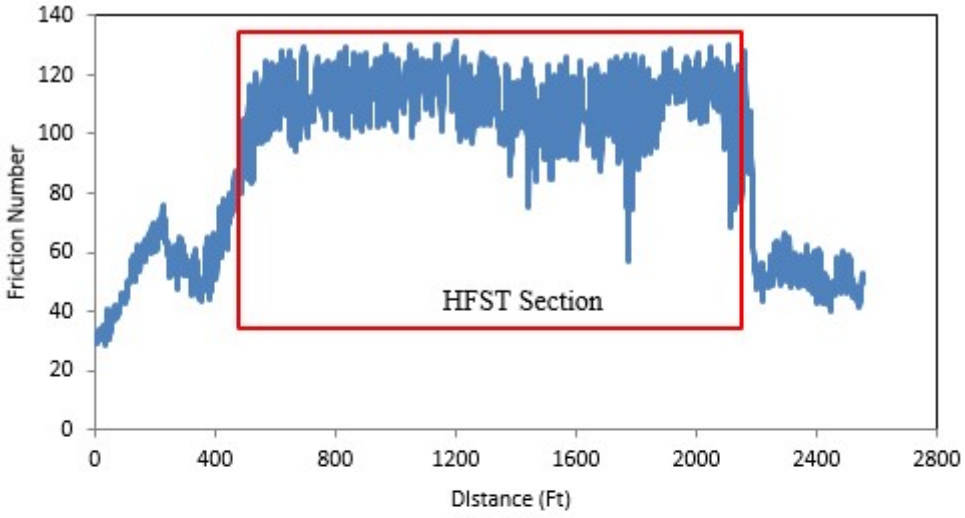

(a) With Distinct Difference

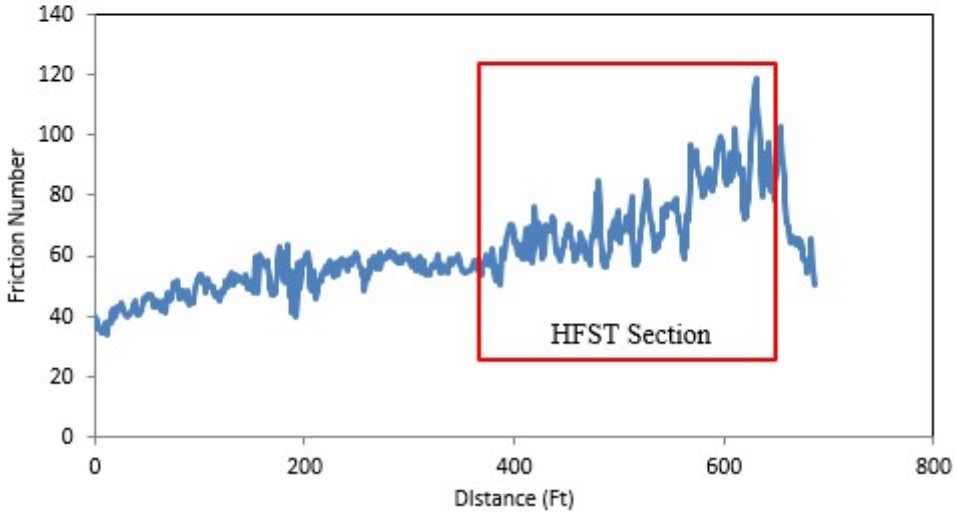

(b) With Minor Difference

Figure 3.2. Example friction data

Pavement Macro-texture

The methodologies for texture measurement can be grouped into two categories: static and high-speed methods. Traditionally the measurement of pavement macro-texture at high-speed is based on single line measurement of longitudinal profile in the wheelpath. Mean Profile Depth (MPD) is one of the widely used texture indexes. Example MPD data plots from the 3D Ultra system are shown in Figure 33. Similar to friction data, some sites exhibit much higher MPD values on HFST surface in contrast to the abutting pavement, while others don't exhibit noticeable differences.

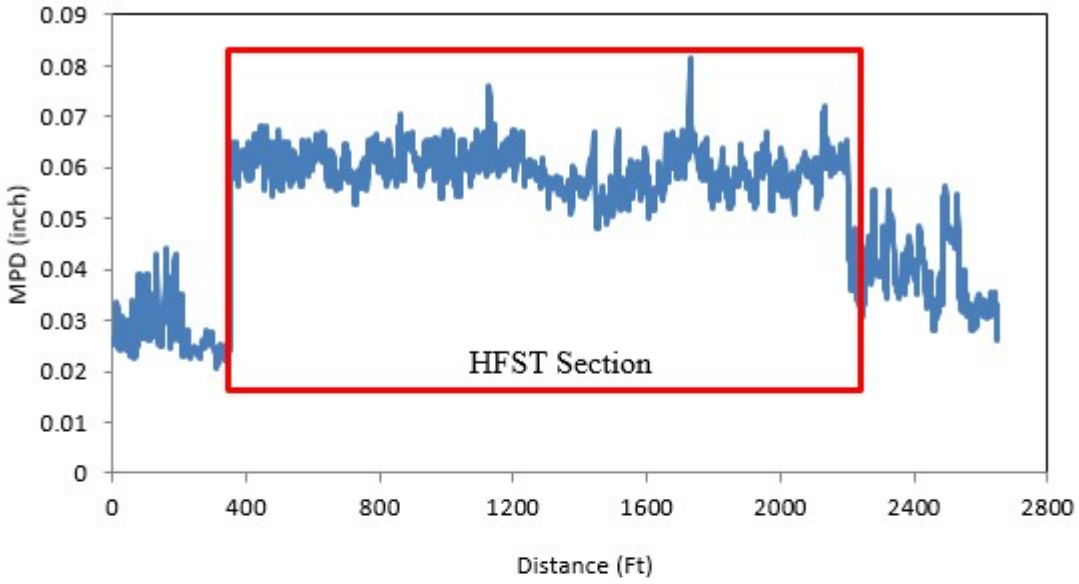

(a) With Distinct Difference

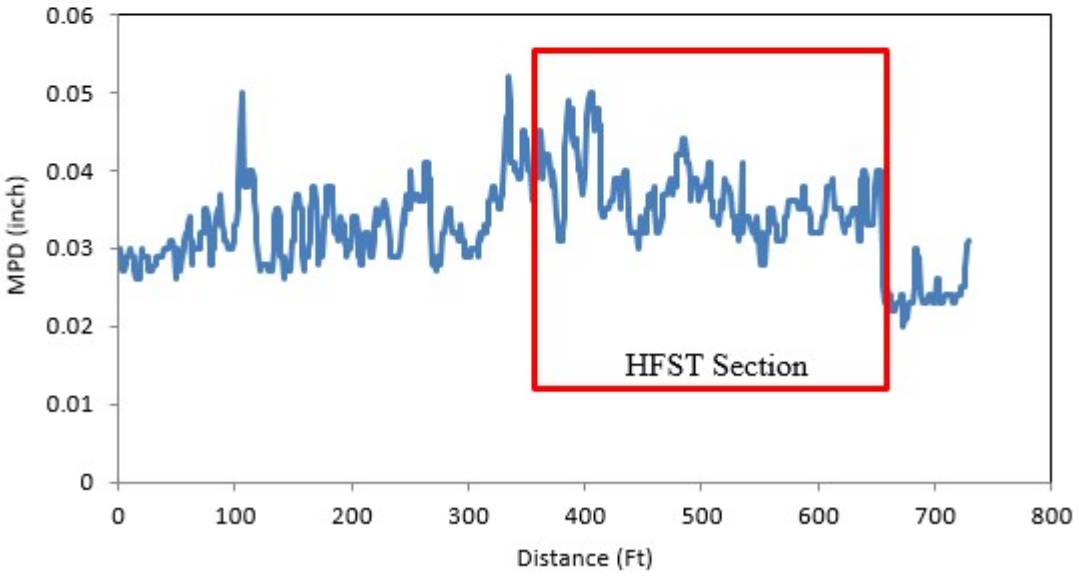

(b) With Minor Difference

Figure 3.3. Example MPD data

Roadway Geometry

The Inertial Measurement Unit (IMU) mounted on the PaveVision3D data collection vehicle can measure the Euler angles, which include roll (Euler angle about x-axis), pitch (Euler angle about y-axis) and yaw (Euler angle about z-axis). The roll angle is widely accepted to represent pavement cross slope, and pitch angle is widely used to represent the pavement longitudinal grade. The cross slope, longitudinal grade and radius of each HFST site are calculated based on collected IMU data.

Evaluation of HFST Effectiveness

The 1mm 3D data are collected 300ft to 500ft before and/or after each HFST section so that the measured surface characteristics before, after, and on the HFST sites can be compared and statistical analyses performed to determine the effectiveness of the HFST sites in improving surface characteristics. The beginning and end locations of each HFST section are determined based on "event markers" manually recorded by the field friction data collection crew, and visually from collected 3D data sets. A paired t-test with equal variance is performed for each HFST site. The t-test investigates the difference between the means of the non-HFST and HFST treatment sections. At 95% confidence interval, if P-value is smaller than 0.05, the null hypothesis is rejected and the mean of the two groups are significantly different.

The friction and MPD data are reported at 1.0 ft interval. The t-test results for friction number (FN) and MPD for each data collection are summarized in Table 3.1. It is evident that HFST surfaces have significantly different friction numbers (with an average P = 0.01 for all the HFST sites) and surface texture MPD values (with an average P = 0.01 for all the HFST sites) than those on the abutting pavement. The average friction number of all HFST sites is 86.76, while the friction of non-HFST surface has an average of 56.56. The average MPD of all HFST sites is 0.0522 inches (1.32 mm), while the MPD of non-HFST surface has an average of 0.0410 inches (1.04 mm).

Table 3.1. Paired t-test results for friction numbers and MPDs

Data Collection ID	FN_{Mean} – HFST	FN_{Mean} – Non-HFST	df	P value	Sig. Diff?	MPD_{Mean} –HFST	MPD_{Mean} – Non-HFST	df	P value	Sig. Diff?
1	98.08	51.79	1060	0	Yes	0.0498	0.0345	1274	0	Yes
2	103.49	58.04	990	0	Yes	0.0514	0.0284	1172	0	Yes
3	87.89	68.3	1540	0	Yes	0.0548	0.0677	1739	0	Yes
4	81.69	70.38	1541	0	Yes	0.0526	0.0581	991	0	Yes
5	107.86	63.86	1477	0	Yes	0.0625	0.0465	1184	0	Yes
6	112.42	63.85	1499	0	Yes	0.0634	0.0459	957	0	Yes
7	104.05	60.55	1088	0	Yes	0.0513	0.0342	978	0	Yes
8	98.74	57.76	984	0	Yes	0.0497	0.0321	1454	0	Yes
9	100.6	55.84	1113	0	Yes	0.0517	0.0346	1075	0	Yes
10	91.35	44.1	826	0	Yes	0.0501	0.03	691	0	Yes
11	102.39	61.77	1019	0	Yes	0.049	0.036	1243	0	Yes
12	94.59	49.12	1194	0	Yes	0.0496	0.0351	1119	0	Yes
13	57.64	43.83	1272	0	Yes	0.0383	0.0283	1132	0	Yes
14	83.17	52.64	768	0	Yes	0.043	0.0192	285	0	Yes
15	65.55	64.93	925	0.38	No	0.0362	0.0217	351	0	Yes
16	64.28	53.3	1677	0	Yes	0.0456	0.0332	1600	0	Yes

Data Collection ID	FN_{Mean} – HFST	FN_{Mean} – Non-HFST	df	P value	Sig. Diff?	MPD_{Mean} –HFST	MPD_{Mean} – Non-HFST	df	P value	Sig. Diff?
17	59.14	52.73	1767	0	Yes	0.0291	0.0289	2143	0.41	No
18	73.12	54.51	831	0	Yes	0.0419	0.0313	616	0	Yes
19	94.98	60.43	791	0	Yes	0.09	0.0825	1181	0.03	Yes
20	72.81	54.5	471	0	Yes	0.0351	0.0323	645	0	Yes
21	68.93	54.32	367	0	Yes	0.0397	0.0257	418	0	Yes
22	64.49	45.09	244	0	Yes	0.0423	0.0812	303	0	Yes
23	64.14	37.95	253	0	Yes	0.0539	0.1083	365	0	Yes
24	84.14	76.23	524	0	Yes	0.0384	0.0498	399	0	Yes
25	52.1	69.09	1940	0	Yes	0.041	0.0356	1308	0	Yes
26	56.5	76.24	1995	0	Yes	0.038	0.0383	1814	0.01	Yes
27	74.62	60.83	900	0	Yes	0.0548	0.0449	844	0	Yes
28	72.79	55.66	267	0	Yes	0.0562	0.0402	859	0	Yes
29	101.45	66.22	310	0	Yes	0.0579	0.0465	429	0	Yes
30	59.5	55.74	414	0	Yes	0.0548	0.0514	769	0	Yes
31	90.25	41.1	2543	0	Yes	0.0572	0.0293	2100	0	Yes
32	93.37	42.45	2561	0	Yes	0.0581	0.027	1981	0	Yes
33	107.81	53.06	1968	0	Yes	0.0592	0.0313	588	0	Yes
34	108.33	55.36	1734	0	Yes	0.0734	0.0382	1376	0	Yes
35	102.6	57.24	1069	0	Yes	0.0671	0.0452	1306	0	Yes
36	92.68	49.37	1635	0	Yes	0.0526	0.0397	1286	0	Yes
37	111.46	51.08	1468	0	Yes	0.0474	0.035	489	0	Yes
38	97.06	54.02	969	0	Yes	0.0692	0.0354	1803	0	Yes
39	124.28	50.44	1962	0	Yes	0.0588	0.0354	1840	0	Yes
40	88.41	58.68	1864	0	Yes	0.0608	0.0381	1054	0	Yes
41	88.32	66.57	1369	0	Yes	0.0663	0.0419	989	0	Yes

Figure 3.4 shows the difference between the two means of friction numbers and MPDs for each HFST data collection. The majority of the HFST sites have much higher friction numbers and MPD values comparing to the non-HFST surfaces. However, there are several exceptions. Sites 25 and 26 have smaller friction numbers on HFST surfaces than those on the non-HFST surfaces. The presence of foreign materials observed on the two HFST locations during data collection may result in the lower friction numbers of the sites. Approximately identical friction numbers are observed for Site 15 on HFST and non-HFST surfaces. In addition, the friction on HFST of Site 30 is slightly higher than that on the non-HFST surface even though the treatment was applied only one year prior to data collection. For MPD, 5 out of 41 collections report smaller MPDs on HFST surfaces, such sections including Sites 3, 4, 22, 23, and 24. It is also observed that over ½ of the flint sites have the lowest FN Ratios.

The comparisons of the average rutting on HFST and non-HFST of asphalt pavement surfaces are shown in Figure 3.5. No consistent statistical conclusion can be made based on the t-test results: some sections have significantly different rutting while others don't between HFST and non-HFST segments. This is logical since HFST treatments do not correct rutting problems on existing pavement surfaces. The rutting on an HFST surface is dependent on the pavement condition before the treatment. The average rutting are 4.24 mm and 4.53 mm for HFST and non-HFST respectively. The average P-value is 0.14, which indicates that on average no significant difference is observed for rutting on non-HFST versus HFST surfaces.

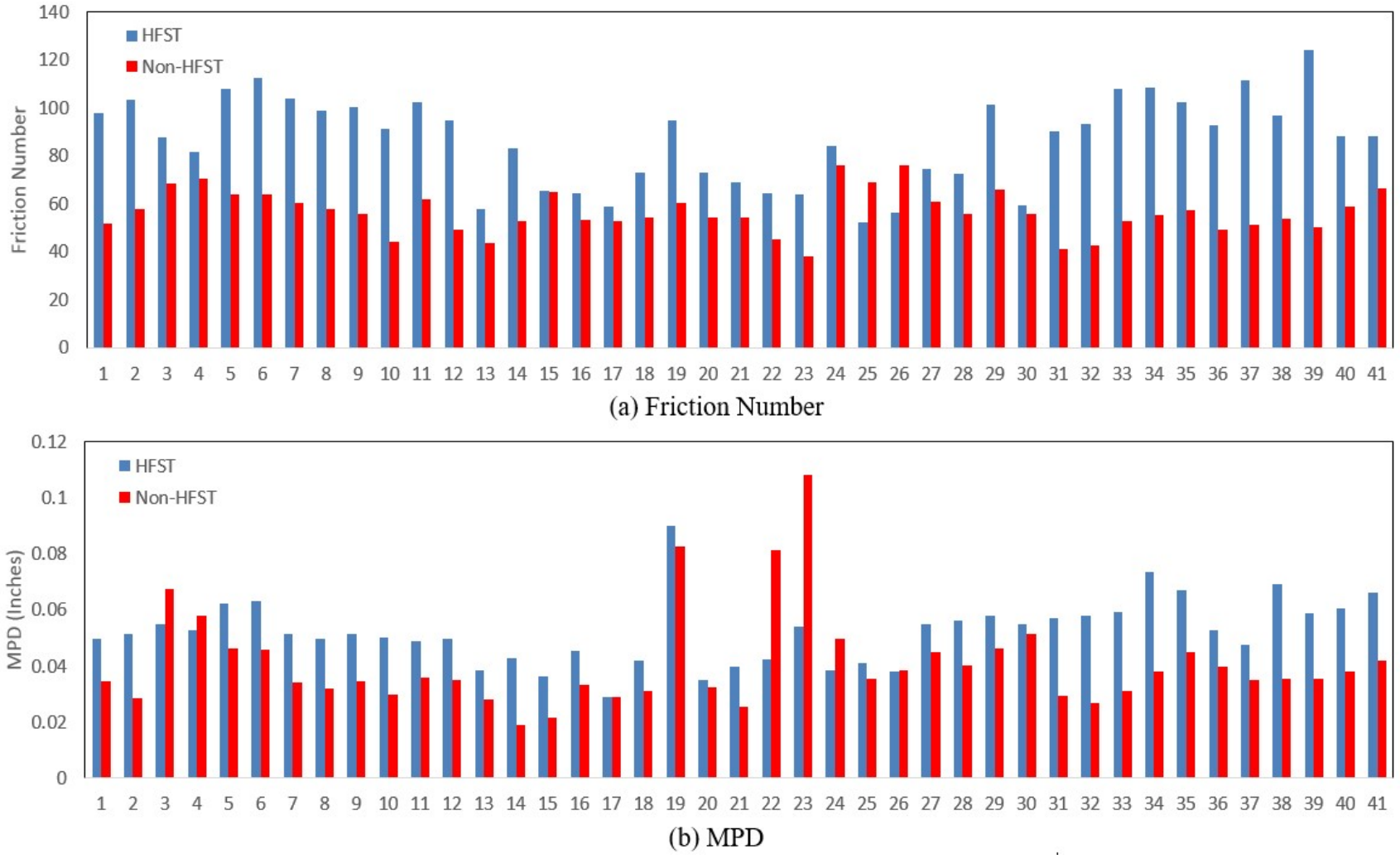

Figure 3.4. Average friction numbers and MPDs for HFST sites

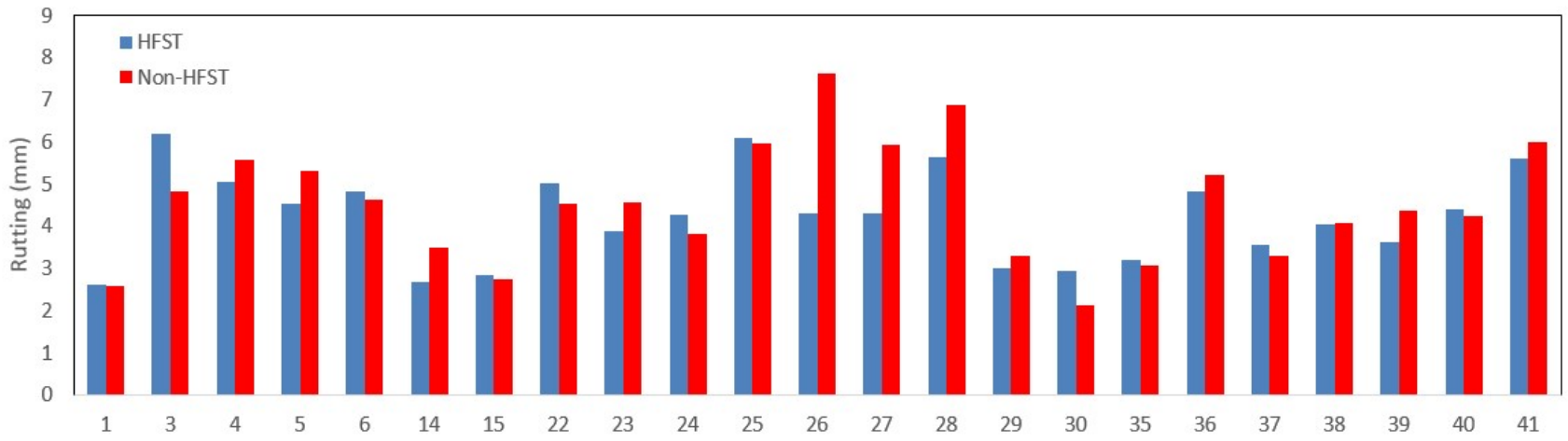

Figure 3.5. Average rutting for HFST sites

HFST Friction Performance

Potential Influencing Factors

Influencing factors relating to pavement friction are generally categorized as pavement surface characteristics, vehicle operational parameters, tire properties, and environmental factors [12]. The influence of asphalt mixture type and Portland cement concrete surface textures on pavement friction has been widely researched [13]. Several pavement friction models have been developed, some of which are established based on macro- and micro-texture of mix aggregates [14]. Operational factors including water film thickness, test speed, or temperature are found to affect friction measurement [15, 16]. Studies also find that temperature could affect pavement friction in short-term and long-term [17, 18, and 19].

Based on data availability in this study, precipitation, average temperature, HFST installation age, aggregate type, and annual average daily traffic (AADT) for each HFST site are identified as the potential influencing factors to evaluate the HFST friction performance in the long-term and at a wider scale. Precipitation and average temperature data are obtained from the climate station close to each HFST site. Two indicators, friction number on HFST (FN_{HFST}) and the ratio of friction number (FN Ratio) are used to evaluate HFST pavement friction performance. Herein, FN Ratio is the friction number on HFST (FN_{HFST}) divided by the friction number on Non-HFST ($FN_{Non-HFST}$).

$$\text{FN Ratio} = \frac{FN_{HFST}}{FN_{Non-HFST}} \quad (3.1)$$

The potential influencing factors and corresponding friction information for each data collection are provided in Table 3.2. FN Ratio, FN_{HFST}, and $FN_{Non-HFST}$ for each data collection are evaluated considering the aforementioned factors:

- As shown in Figure 3.6, FN Ratio and FN_{HFST} show decreasing trend with the increase of HFST installation age and average temperature.
- Based on the data trend shown in FIG, 6(B), when HFST sites are approximately 60 month of installation age, FN Ratio approaches approximately 1.0, which indicates in general that the average life of a HFST surface is around 5 years and the benefit of HFST in friction effectiveness is nearly lost by that time. However, it should be emphasized that this observation is solely based on the monitoring data from a limited number of HFST sites included in this study. Moreover, all the sites that are 60 months or older are constructed using flint as the aggregates.
- HFST sites installed with calcined bauxite aggregates exhibit better friction performance than those with flints (Figure 3.7).
- No trend is observed between friction performance (FN Ratio and FN_{HFST}) and precipitation, AADT respectively, neither does the accumulated traffic repetitions (which is AADT times 365 days and HFST installation age).
- There is no obvious relationship between $FN_{Non-HFST}$ and the five influencing factors.

In warmer region, higher temperature may leads to softer polymeric resin binder compared with that in colder region, and generates lower FN Ratio and FN_{HFST}. As time goes by, older installation endures more influence of traffic wear and environment, therefore lower FN Ratio and FN_{HFST} come with older HFST sections. AADT should have an impact on pavement friction development since pavement wears and friction values decrease with repetitive traffic applications. However,

the majority of the HFST sites are located either on ramps or multiple-lane highways. Detailed traffic data on ramps and for each lane of multiple-lane sections are not available and the AADT values have to be estimated based on engineering judgment. With more accurate traffic data, the relationship between AADT and friction may be better revealed.

Table 3.2. Potential influencing factors of HFST friction performance

Data Collection ID	Precip. (Inch)	Air Temp. (°F)	Data Collection Speed (MPH)	Install. Age (Month)	Aggregate	AADT	FN_{HFST}	FN Ratio
1	48.4	53.1	30	4	Bauxite	6400	98.08	1.89
2	48.4	51.7	30	4	Bauxite	9810	103.49	1.78
3	37.7	86.2	40	30	Bauxite	13500	87.89	1.29
4	37.7	85.2	40	30	Bauxite	13500	81.69	1.16
5	55.4	43.8	40	17	Bauxite	2100	107.86	1.69
6	55.4	44	40	17	Bauxite	2100	112.42	1.76
7	34.6	51.3	40	30	Bauxite	14167	104.05	1.72
8	34.6	51.8	40	30	Bauxite	14167	98.74	1.71
9	34.6	51.9	40	30	Bauxite	14167	100.60	1.80
10	34.6	51.4	40	30	Bauxite	14167	91.35	2.07
11	34.6	52.3	40	30	Bauxite	14167	102.39	1.66
12	34.6	51.8	40	30	Bauxite	14167	94.59	1.93
13	35.5	33.9	40	64	Flint	26165	57.64	1.32
14	35.5	33.7	30	64	Flint	1717	83.17	1.58
15	35.5	33.8	30	64	Flint	1717	65.55	1.01
16	34.3	36.5	40	64	Flint	6350	64.28	1.21
17	30.7	44.5	30	51	Flint	10510	59.14	1.12
18	34	50.8	30	51	Flint	4291	73.12	1.34
19	30.2	41.7	30	51	Bauxite	3300	94.98	1.57
20	30.2	44.3	30	51	Bauxite	3400	72.81	1.34
21	30.2	44.2	30	51	Bauxite	3400	68.93	1.27
22	30.2	49.4	20	51	Bauxite	2750	64.49	1.43
23	30.2	45.1	20	51	Bauxite	2750	64.14	1.69
24	12.8	38.5	30	63	Flint	2760	84.14	1.10
25	14	39	40	63	Flint	5955	52.10	0.75
26	14	38.5	40	63	Flint	5955	56.50	0.74
27	44	58.6	30	9	Bauxite	1300	74.62	1.23
28	44	58.6	30	9	Bauxite	1300	72.79	1.31
29	44	55.8	30	9	Bauxite	1300	101.45	1.53
30	44	55.3	30	9	Bauxite	1300	59.50	1.07
31	27.2	50	40	4	Bauxite	400	102.60	1.79
32	27.2	50.9	40	4	Bauxite	400	92.68	1.88
33	27.2	50.7	40	4	Bauxite	400	111.46	2.18
34	27.2	37.5	40	4	Bauxite	1720	97.06	1.80
35	27.2	37.8	40	4	Bauxite	1720	124.28	2.46
36	26.4	31.4	40	4	Bauxite	8420	90.25	2.20
37	26.4	32.1	40	4	Bauxite	8420	93.37	2.20
38	26.4	32.4	40	4	Bauxite	8420	107.81	2.03
39	26.4	31.9	40	4	Bauxite	8420	108.33	1.96
40	36.8	47	40	39	Bauxite	15500	88.41	1.51
41	36.8	46.3	40	39	Bauxite	15500	88.32	1.33

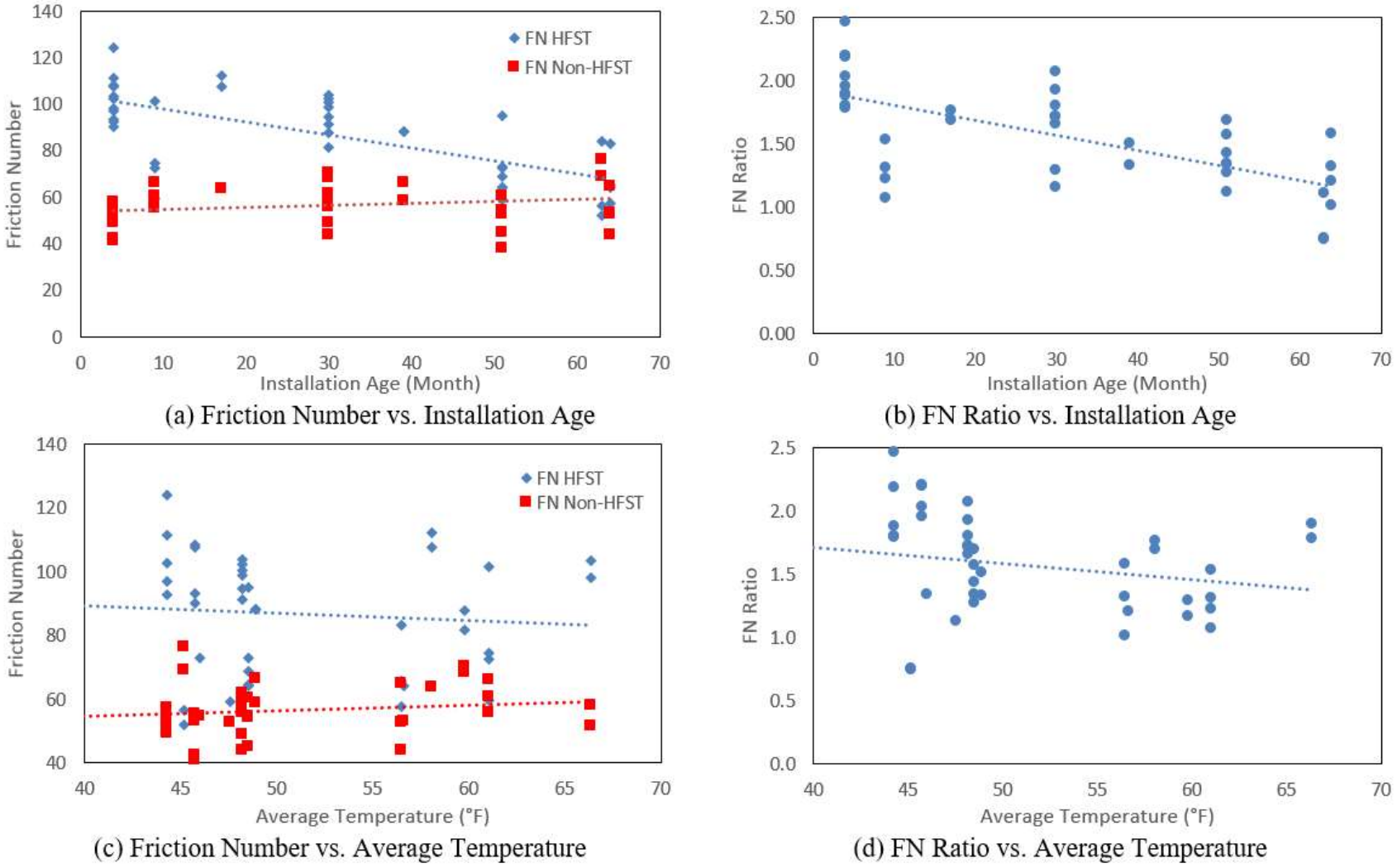

Figure 3.6. HFST friction performance vs. installation age and average temperature

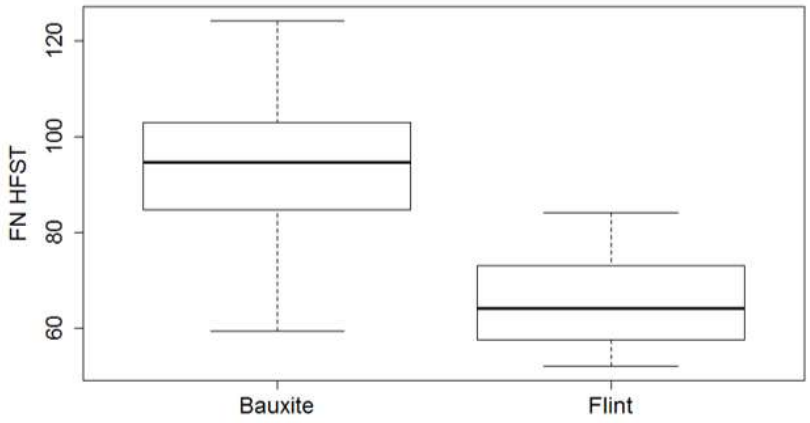

(a) FN_{HFST} vs. Aggregate Type

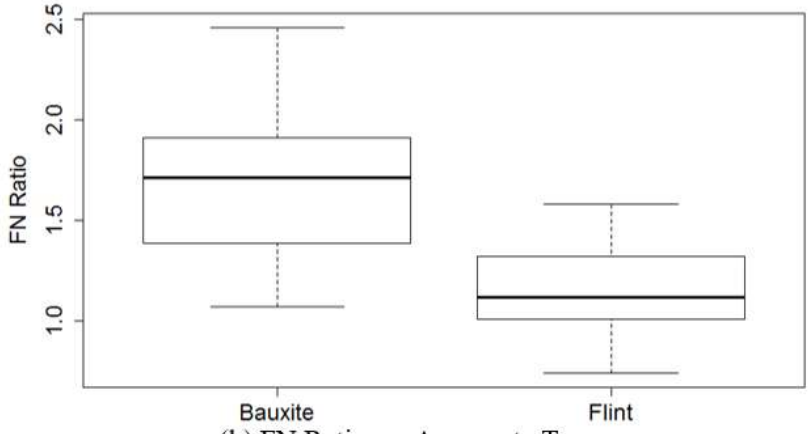

(b) FN Ratio vs. Aggregate Type

Figure 3.7. HFST friction performance vs. aggregate type

Multivariate Analysis Results

Multivariate analysis is conducted to analyze the effect of the influencing variables on FN Ratio, FN_{HFST}, and $FN_{Non\text{-}HFST}$. Precipitation, average temperature, HFST installation age, AADT are continuous independent variables, while aggregate type is a categorical variable and should be properly coded and quantified before multivariate analysis could be performed. Herein bauxite aggregate is represented as '1' while flint is coded as '0' in data preparation of model development. P-value is used to evaluate the significant level of each influencing variable on the dependent outcomes (which are the two friction performance measures). The multivariate analysis result is shown in Table 3.3.

At 95% confidence interval, if P-value is smaller than 0.05, the corresponding variable has significant effect on the dependent variables. The P-values for average temperature and HFST installation age are much smaller than 0.05, which means they have significant effect on FN Ratio and FN_{HFST}. The corresponding coefficient of those two dependent variables are negative, which indicates that FN Ratio and FN_{HFST} decrease as those two variables increase. P-value of aggregate type (larger than 0.05) shows that it is not a significant factor for FN Ratio and FN_{HFST}. However the corresponding coefficients of aggregate type are positive, which implies HFST using bauxite (coded as '1') will add a positive number into the predicted FN Ratio or

FN_{HFST} while HFST using flint (coded as '0') doesn't include such positive contribution to friction numbers. This statistic results support the data shown in Figure 3.8 that FN Ratio and FN_{HFST} for HFST using bauxite are generally greater than those using flint. For $FN_{Non\text{-}HFST}$, P-values for all the five variables are greater than 0.05, which indicates that the independent variables have insignificant impacts on pavement friction for non-HFST sections.

Table 3.3. Multivariate analysis results (considering all five independent factors)

Variables	FN Ratio Coefficients	FN Ratio P-value	FN HFST Coefficients	FN HFST P-value	FN Non-HFST Coefficients	FN Non-HFST P-value
Intercept	3.113	0.000	146.258	0.000	40.368	0.012
Precipitation (Inch)	0.016	0.074	1.027	0.020	-0.210	0.495
Average Temperature (°F)	-0.037	0.003	-1.626	0.005	0.459	0.250
Installation Age (Month)	-0.011	0.000	-0.473	0.001	0.061	0.523
Aggregate	0.064	0.684	1.978	0.791	-1.517	0.780
AADT	0.000	0.265	0.000	0.462	0.000	0.619

Table 3.4. Multivariate analysis results (considering only the two significant factors)

Variables	FN Ratio Coefficients	FN Ratio P-value	FN HFST Coefficients	FN HFST P-value	FN Non-HFST Coefficients	FN Non-HFST P-value
Intercept	2.912	2.62E-10	130.027	2.07E-09	42.056	0.000
Average Temperature (°F)	-0.019	0.006	-0.507	0.111	0.229	0.272
Installation Age (Month)	-0.013	1.05E-07	-0.575	4.07E-07	0.094	0.141

Subsequently, multivariate analysis considering only the two significant influencing factors (average temperature and installation age) is conducted and the results are appended in Table 3.4. Both factors remain to be significant for the prediction of FN Ratio. However, the P-value of average temperature on FN_{HFST} is larger than 0.05, which indicates that the impact of average temperature on FN_{HFST} is not as significant as that of installation age, which supports the data shown in Figure 3.6(c) that FN_{HFST} decreasing trend is not as significant as that of installation age. The multiple linear regression models are therefore developed as shown in Equation (3.2) to predict FN Ratio and FN_{HFST}:

$$FN\ Ratio = 2.912 - 0.019 * Average\ Temperature - 0.013 * Age$$
$$FN_{HFST} = 130.027 - 0.507 * Average\ Temperature - 0.575 * Age \quad (3.2)$$

The predicted and measured FN Ratio and FN_{HFST} for all the 41 data collections are plotted in Figure 3.8. The predictions follow similar development trend as the actual measured FN Ratio and FN_{HFST}, and the R-squared values are 0.55 and 0.50 respectively. There are several potential reasons may cause the moderate R-squared values. Several factors of many HFST sites may take the same values, which reduces the variability of the data sets. For example, if HFST sites are close to each other in distance, the climate data for these sites are obtained from one weather station and the same values of precipitation and average temperature are used. For HFST sites

with multiple lanes, AADT data remains the same for the site for all lanes. More detailed and accurate data could result in better friction prediction models with higher R-squared values.

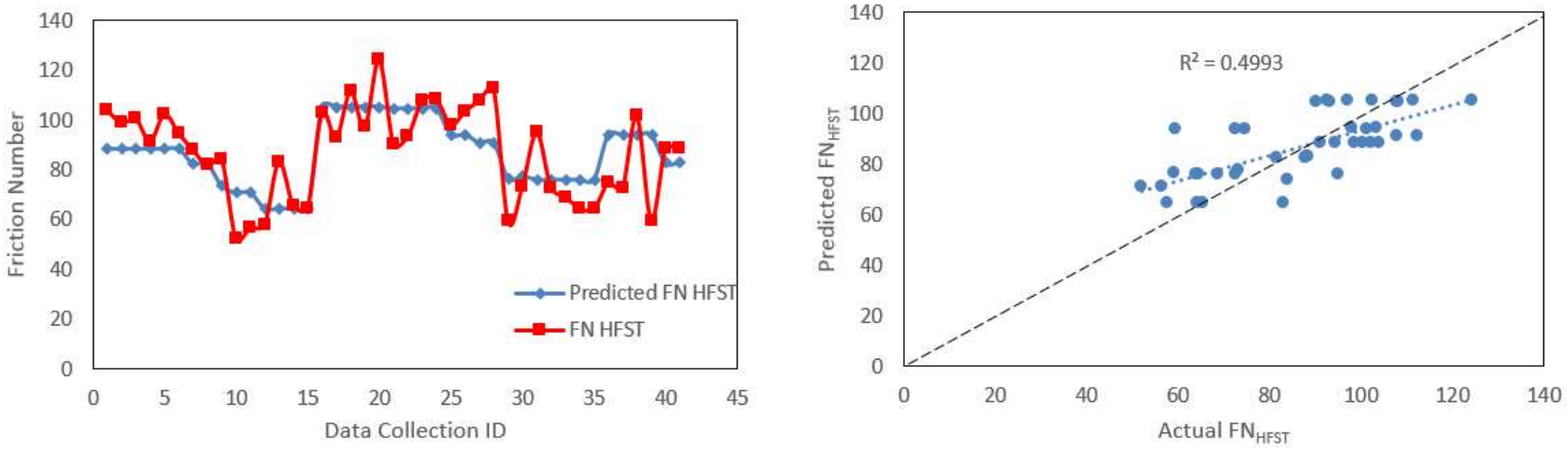

(a) Predicted vs. Measured FN_{HFST}

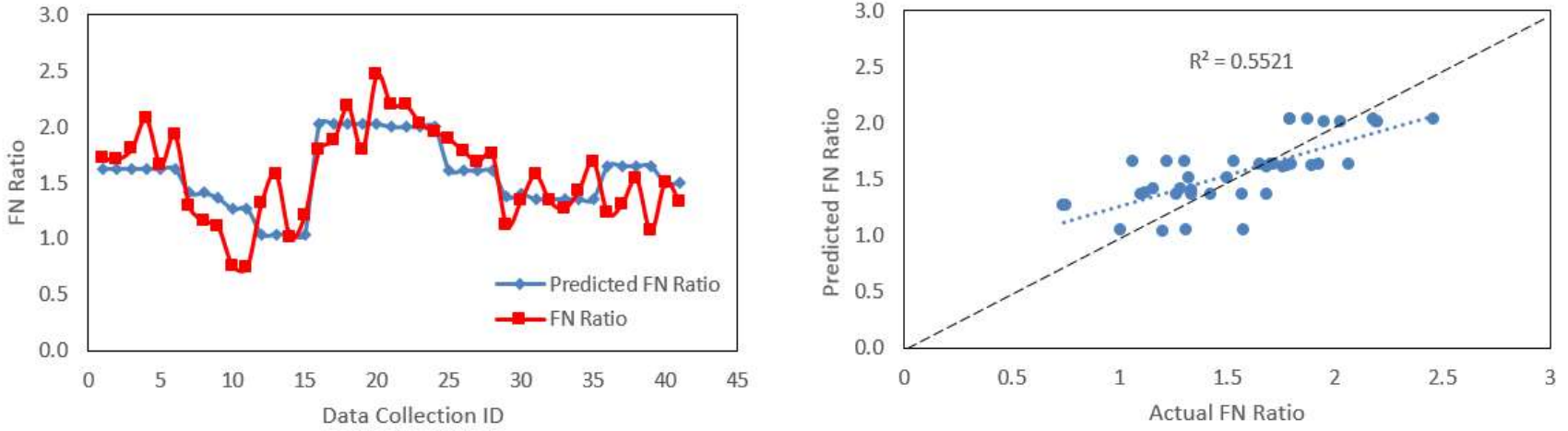

(B) Predicted vs. Measured FN Ratio

Figure 3.8. HFST friction performance prediction

4. GEOMETRIC TEXTURE INDICATORS FOR SAFETY ANALYSIS

Introduction

Pavement surface texture is defined as the deviation of the pavement surface from a true planar surface or an ideal shape [20]. These deviations occur at several distinct levels of scale, each defined by wavelength (λ) and peak to peak amplitude (A) of its components. Per the texture definition by Permanent International Association of Road Congresses (PIARC), pavement surface texture can be divided into four categories [12, 21]: 1) Micro-texture ($\lambda < 0.5$ mm, $A \in$ [1 to 500 μm]); 2) Macro-texture ($\lambda \in$ [0.5 to 50 mm], $A \in$ [0.1 to 20 mm]); 3) Mega-texture ($\lambda \in$ [50 to 500 mm], $A \in$ [0.1 to 50 mm]); 4) Roughness or unevenness (λ>500 mm).

It is widely recognized that pavement surface texture affects many different pavement–tire interactions [22, 23]. Wet pavement friction, interior and exterior noise, splash and spray are mainly dependent on macro-texture properties. Dry pavement friction and tire wear are highly associated with micro-texture characteristics. Other tire-pavement interactions e.g. rolling resistance and ride quality are affected by the mega-texture and roughness. Therefore the study on macro-texture property places a vital role in evaluating pavement safety performance. In this study texture indicator is defined as an index or parameter to represent attributes of pavement surface texture.

Currently several texture indicators have been used to characterize pavement surface texture. Mean Profile Depth (*MPD*) is the one of the commonly used texture indicator measured using the Circular Track Meter [24] or other laser based measuring systems [25]. The other standardized index is Mean Texture Depth (*MTD*), which is either measured using Sand Patch Method [26] or transformed via MPD [25]. Root Mean Square (*RMS*) is measured by several data collection systems, and it can be used as an indicator to represent the amplitude distribution of profile elevations [27, 28]. In addition, some other texture indicators such as Hessian Model [29], Power Spectral Density (*PSD*) [30], and Fractal Dimension (*FD*) [31] are also explored to characterize pavement surface texture. However, these parameters only disclose partial aspects of surface texture properties, e.g. *MPD* only reflects the height property of pavement surface.

Pavement friction is a measure of the force generated when a tire loses traction on a pavement surface, and is dependent on a large number of factors including road types, tire properties, vehicle suspension system, traveling speed, ambient temperature, and the presence of contaminants such as oil and water [12]. Skid resistance is the contribution of roadway surface texture to form or develop this friction, and its value relies on the interaction between pavement surface and vehicle tires. The measurement of skid resistance is a process for monitoring pavement safety performance and preventing crashes on wet roadways. However, frictional measurement devices are relatively complex and costly to operate and maintain. During data collection, in most cases a truck carrying a large water tank is needed to saturate pavement surface with a prescribed layer of water during measurements, which is challenging for network level pavement friction measurement, so the estimation of skid resistance is becoming increasingly of interest [16, 32-35].

Over the years, many studies have been performed to investigate the relationships between texture indicators and frictional indexes, some of which attempt to establish acceptable mathematical models to correlate skid resistance with texture characteristics [13, 36-44]. However, there are several limitations on the use of the existing models to predict pavement friction with texture data in the project- or network- level pavement safety surveys due to the two factors: 1) models are developed in laboratories with good correlations using high resolution data that are normally difficult to acquire in the field; 2) models are developed in fields with low correlations using one single line measurement of profile data, primarily in terms of *MPD*. Therefore there is a need to develop a reliable model for network level pavement friction survey based on improved texture data with broader pavement surface coverage using a wide range of texture indicators.

Geometric Texture Indicators

In the past decades several surface characterization techniques have been proposed for various application, and are generally grouped into two categories: scale-dependent and scale-independent, as shown in Figure 4.1 [45, 46].

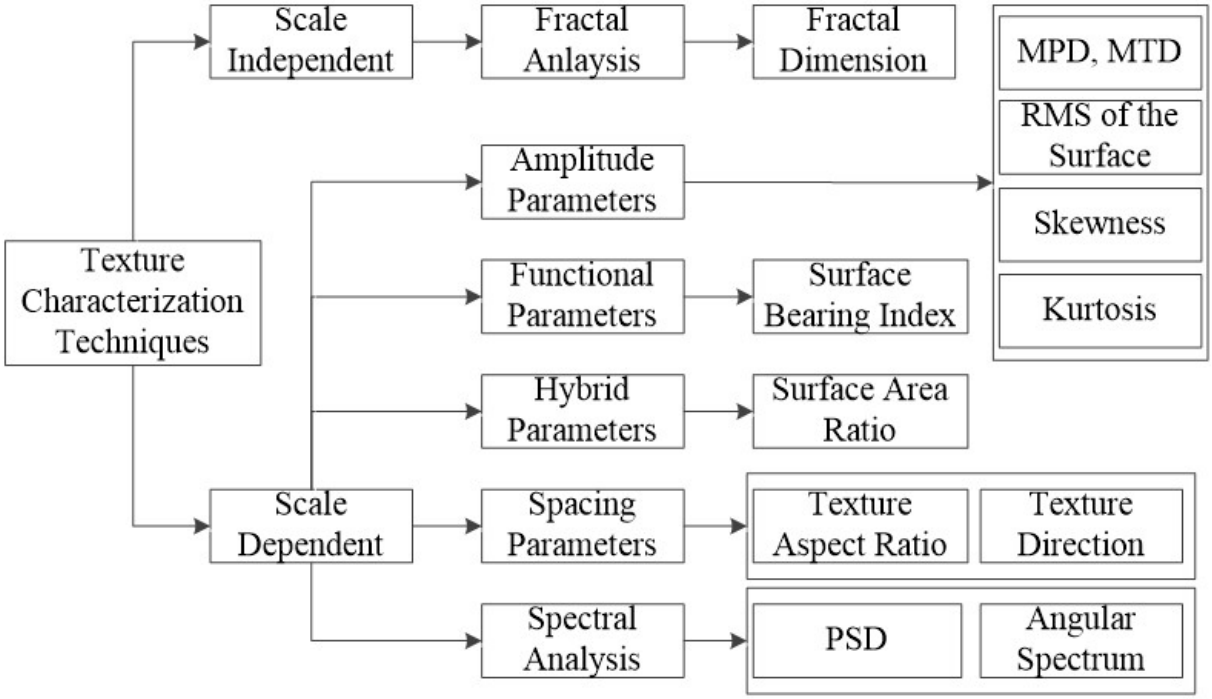

Figure 4.1. Schematic diagram of pavement surface characterization techniques

The scale-independent parameters indicate texture characterization results are independent of the measurement scales (data resolution). Fractal analysis based indicator falls into this category. The scale-dependent parameters mean texture characterization results are dependent on the measurement scales. In other words, the analysis results might be quite different when different measurement scales are used. The scale-dependent parameters can be grouped into five categories: amplitude parameters, functional parameters, spectral analysis, spacing (or spatial) parameters, and hybrid parameters [45].

In this study the four scale-dependent parameters (amplitude, spacing, hybrid, and functional parameters), also termed as geometric texture indicators, are used as the dependent variables to estimate pavement friction. To avoid the use of the two highly correlated texture indicators, the relationships among these texture indicators are investigated as well. Finally pavement safety property in terms of pavement friction is evaluated through a mathematical model developed from the geometric texture indicators.

Amplitude or Height Parameters

Amplitude parameter only considers the height or elevation information of surface texture, while ignores the impacts of data spacing on texture properties. For amplitude-related parameters, five texture indicators namely *MPD*, *MTD*, *RMS*, *Skewness*, and *Kurtosis* are presented [45, 46].

Mean Profile Depth (MPD)

MPD is a widely accepted and used texture indicator. It is defined as the average of all mean segment depths of all segments of the profile. According to the *MPD* computation practice [21, 25], the calculation of *MPD* can be described as follows: the measured profile is divided into different segments which have a length of 100±2 mm, then the segment is divided in two equal halves and the height of the highest peak in each half segment is determined. The average of these two peak heights minus the average of all heights is the mean segment depth. The average value of the mean segment depths for all segments making up the measured profile is reported as the *MPD*, as illustrated in Figure 4.2.

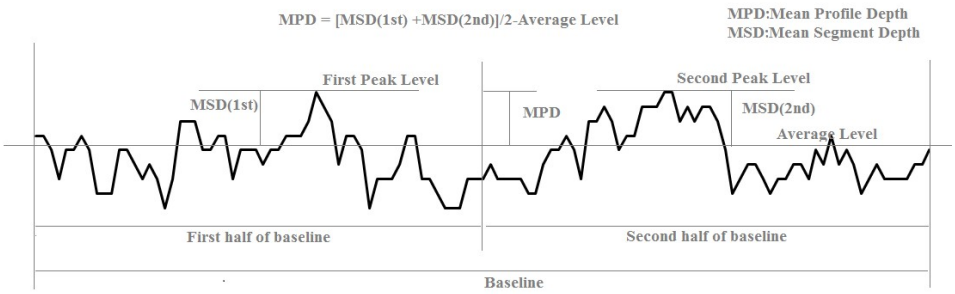

Figure 4.2. A general procedure for MPD calculation

Simulated Mean Texture Depth (SMTD)

MTD can be viewed as a representation of 3D surface characteristics because it is obtained using volumetric measuring technique [26]. The measured result can be reported as the ground truth. Generally *MTD* can be either measured in field or transformed from *MPD* [25, 26]. However, in this study the *MTD* would be calculated with image processing techniques in the 3D domain [47].

A 3D digital image is composed of many discrete height data which are stored in computers as 2D matrix. Assume the sampled pavement surface data can be divided into several areas; each area has a size of N x M mm, and the *SMTD* can be computed using Equation (4.1):

$$SMTD = \frac{\iint_0^D [F_0 - F(x,y)]dxdy}{D} = \frac{\sum_{x=1}^{N}\sum_{y=1}^{M}[F_0 - F(x,y)]}{D} \quad (4.1)$$

Where: $F(x,y)$- the eight information at point *(x, y)*, D - the integral area which equals to the M x N pixels, F_0- the height value being equivalent to the maximum peak in each area D *(*M x N pixels)

Root Mean Square (RMS)

RMS is a general measurement of surface texture deviation property. If a larger *RMS* is measured on pavement surface, it indicates there is a significant deviations in surface texture characteristics [45]. This parameter can help interpret contact areas between vehicle tires and pavement surface, and thus is highly associated with surface bearing capacity. Its calculation can be mathematically described with Equation (4.2):

$$S_q = \sqrt{\iint_0^D [z(x,y)]dxdy} = \sqrt{\frac{\sum_{x=1}^{N}\sum_{y=1}^{M} z(x,y)^2}{M \times N}} \quad (4.2)$$

Where: M - the number of points per profile, N - the number of profiles, $z(x,y)$- the elevation difference between point (x,y) and the mean plane, S_q - the root mean square of the surface.

Skewness (Ssk) and Kurtosis (Sku)

Skewness and Kurtosis are used to represent 3D surface texture height distribution properties. Figuratively, a histogram of the heights of all measured points is computed. The symmetry and deviation from an ideal Normal Distribution is represented by *Ssk* and *Sku*, and their mathematical descriptions are given as Equations **Error! Reference source not found.**(4.3) and (4.4) [45]:

$$Ssk = \frac{\iint_0^D [z(x,y)^3]dxdy}{S_q^3} = \frac{\sum_{x=1}^{N}\sum_{y=1}^{M} z(x,y)^3}{M \times N \times S_q^3} \quad (4.3)$$

$$Sku = \frac{\iint_0^D [z(x,y)^4]dxdy}{S_q^4} = \frac{\sum_{x=1}^{N}\sum_{y=1}^{M} z(x,y)^4}{M \times N \times S_q^4} \quad (4.4)$$

Where: M - the number of points per profile, N - the number of profiles, $z(x,y)$ - the elevation difference between point (x,y) and the mean plane, S_q - root mean square of the surface. *Ssk* represents the degree of symmetry surface heights about the mean plane. The sign of *Ssk* indicates the predominance of peaks (*Ssk* > 0) or valley structures (*Ssk* < 0) comprising the surface. *Sku* indicates the presence of the inordinately high peaks/deep valleys (*Sku* >3.00) making up the texture. If surface heights are normally distributed, then *Ssk* is 0.00 and *Sku* is 3.00. Similarly, surface heights are positively skewed (*Ssk* > 0) or negatively skewed (*Ssk* < 0). Surface height distributions can be considered as the slow variation (*Sku* < 3) or extreme peaks or valleys (*Sku* > 3). The less the *Sku* is, the smaller the height variation is. The larger the *Sku* is, the larger the height variation is.

Spacing or Spatial Parameters

Texture on pavement surface may have anisotropic or isotropic patterns. Autocorrelation Function (*ACF*) is one of the most effective and robust approach for texture pattern recognition [45]. The *ACF* is determined by taking a duplicate surface $Z((x-\nabla x),(y-\nabla y))$ of the measured surface $Z(x,y)$ with a relative lateral displacement $(\nabla x,\nabla y)$and mathematically multiplying the two surfaces. Subsequently, the resulting function is integrated and normalized to yield a measure of the degree of overlap between the two functions. The *ACF* is a measure of how similar the texture is at a given distance from the original location.

Generally the *ACF* of the anisotropic pavement surface has the fastest decay along the direction perpendicular to the predominant texture direction and the slowest decay along the texture direction, as shown in Figure 4.3a. The *ACF* of isotropic pavement surface has the similar texture aspects in all direction, so it is difficult to determine the fastest and slowest decay of the test sample, as shown in Figure 4.3b. For isotropic pavement surface, it is impossible to normalize the *ACF* of the fastest and slowest decay to 0.2 that is a threshold to determine the fastest and slowest decay.

Figure 4.3. Spatial parameters (a) anisotropic; (b) isotropic

Texture Aspect Ratio (*TAR*) is a measure of the spatial isotropy or directionality of the surface texture. The length of fastest decay is a measure of the distance over the surface such that the new location will have minimal correlation with the original location. On the other hand, the length of the slowest decay is a measure of the distance over the surface such that the new location will have maximum correlation with the original location. The *TAR* is computed as the ratio of the length of fastest decay to the length of the slowest decay, as mathematically described in Equation **Error! Reference source not found.**:

$$0 < TAR = \frac{\text{The distance that the nomalised ACF has the fastest decay to 0.2 in any possible direction}}{\text{The distance that the nomalised ACF has the slowest decay to 0.2 in any possible direction}} \leq 1 \quad (4.5)$$

In principle, the texture aspect ratio has a value between 0 and 1. Larger values, say *TAR*>0.5, indicate stronger isotropic or uniform texture aspects in all directions, whereas the smaller values, say *TAR* <0.3, indicate the stronger periodic texture properties.

Hybrid Parameters

Hybrid parameter is used to overcome some weaknesses of amplitude and spatial parameters. Its calculation depends on both the height and spacing information, and thus any changes that occur in either amplitude or spacing may have an effect on the hybrid property [45, 46]. This parameter

can be computed as: the ratio of the interfacial area of a surface over the sampling area. The areal element can be expressed using the smallest sampling quadrilateral ABCD, as shown in Figure 4.4.

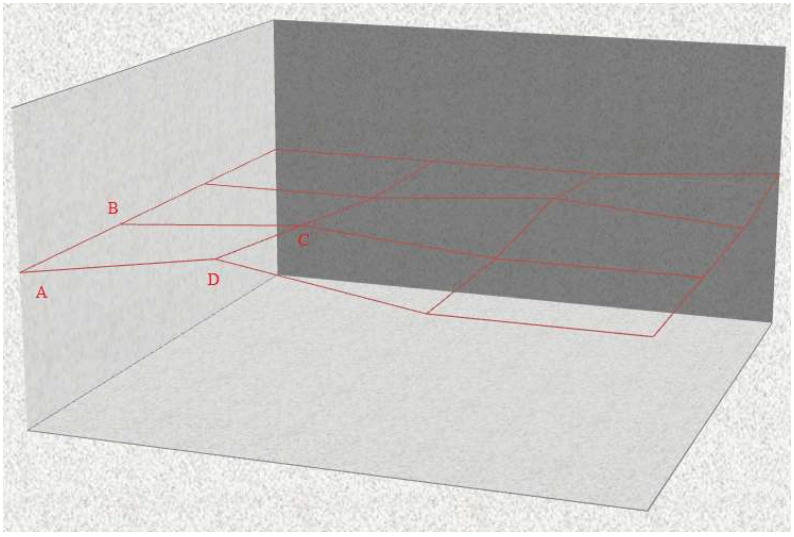

Figure 4.4. Schematic diagram of the interfacial area

Since the four corners of the quadrilateral may not be on the same plane, the interfacial area of the pile-up element may be considered to consist of two triangles, either ABC &ACD or ABD &BCD. The interfacial area of the quadrilateral is defined as an average of two sets of triangle areas (ABC &ACD and ABD&BCD) and its computation principle is given by Equation (4.6):

$$A_{ij} = \frac{1}{4}\left(\left|\overrightarrow{AB}\right| + \left|\overrightarrow{CD}\right|\right)\left(\left|\overrightarrow{AD}\right| + \left|\overrightarrow{BC}\right|\right) = \frac{1}{4}\left\{\left(\left[\Delta y^2 + \left(f(x_i, y_j) - f(x_i, y_{j+1})\right)^2\right]^{\frac{1}{2}} + \left[\Delta y^2 + \left(f(x_{i+1}, y_{j+1}) - f(x_{i+1}, y_{j+1})\right)^2\right]^{\frac{1}{2}} + \left[\Delta x^2 + \left(f(x_i, y_j) - f(x_{i+1}, y_j)\right)^2\right]^{\frac{1}{2}} + \left[\Delta x^2 + \left(f(x_i, y_{j+1}) - f(x_{i+1}, y_{j+1})\right)^2\right]^{\frac{1}{2}}\right)\right\} \quad (4.6)$$

The total interfacial area on the surface can be computed using Equation (4.7):

$$A = \sum_{j=1}^{N-1}\sum_{i=1}^{M-1} A_{ij} \quad (4.7)$$

Then the calculation of surface areal ratio is given as Equation (4.8):

$$SAR = \frac{(A-(M-1)(N-1)\times\Delta x\times\Delta y)}{(M-1)(N-1)\times\Delta x\times\Delta y} \quad (4.8)$$

The developed interfacial area ratio reveals the hybrid property of surfaces. A large value indicates the significance of either the amplitude or the spacing or both.

Functional Parameters

The functional parameters are highly related to their functions i.e. wearing or friction. In this study Surface Bearing Index (*SBI*) was found to have a very close relation with the wearing properties of the surface [45], and equals to the ratio of the root mean square to the surface height at a 5% bearing area, as described using Equation (4.9).

$$SBI = \frac{\sqrt{\iint_0^D [z(x,y)]dxdy}}{H_{5\%}} = S_q / H_{5\%} \quad (4\text{-}9)$$

Where S_q- root mean square; $H_{5\%}$ - the surface height at 5% bearing area.

Correlation Analysis

Relationships among the geometric texture indicators are explored in this study. If the two texture indicators have a high correlation with the R^2 value greater than 0.8, one of them is excluded since they reveal the similar texture properties. However, for two texture indicators having a poor correlation (e.g. $R^2 \leq 0.6$), both are considered to include two different texture properties, and thus the two texture indicators are kept in the model development.

Two groups of samples are chosen to examine the relationships among different geometric texture indicators. The first sample group includes six test specimens. Each specimen is constructed with a different texturing technique. Figure 6a demonstrates the six rigid pavements with turf dragged texture (Figure 4.5a), transversely tined texture (Figure 4.5b), longitudinally tined texture (Figure 4.5c), longitudinally grooved texture (Figure 4.5d), transversely grooved texture (Figure 4.5e), and Next Generation Concrete Surface (NGCS) (Figure 4.5f).

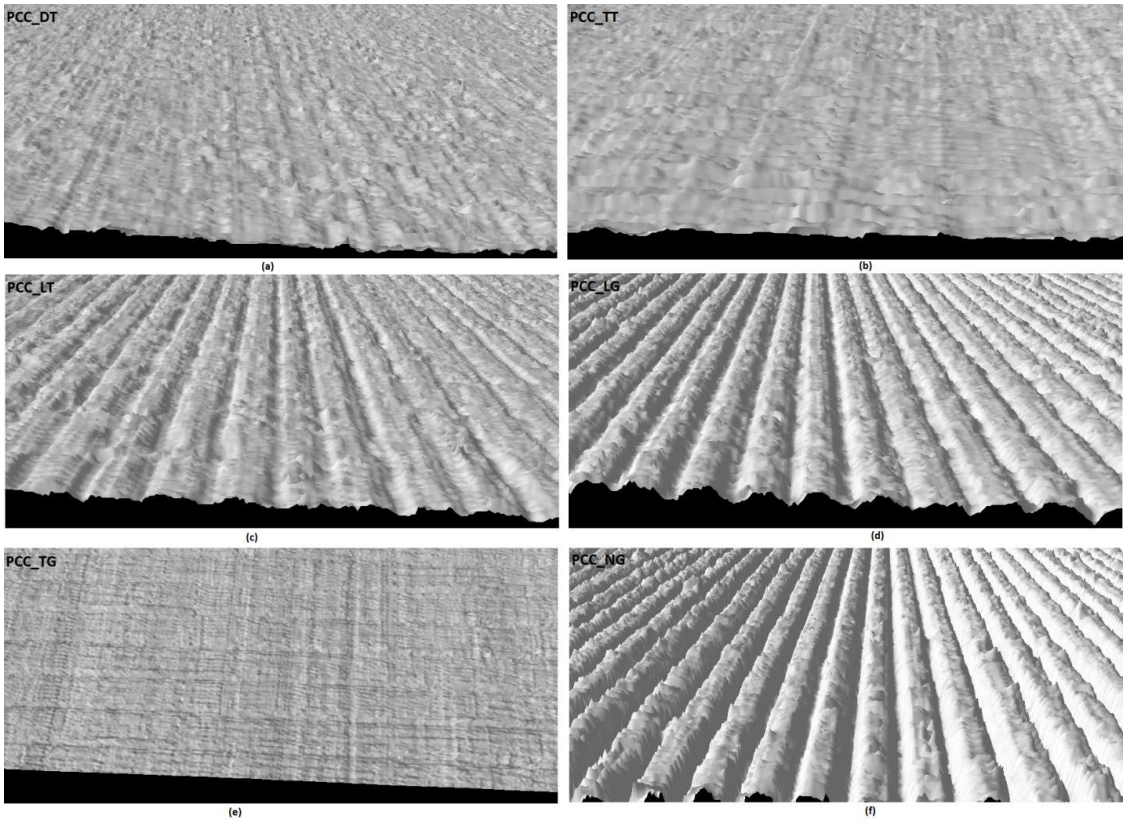

Figure 4.5. 3D rendering of rigid pavement test specimens from 3D Ultra

The second sample group contains three test specimens. Each specimen has obvious different texture properties: AC pavement constructed with dense graded surface (Figure 4.6a), AC pavements with exposed aggregate surface (Figure 4.6b), and high friction treated surface (Figure 4.6c).

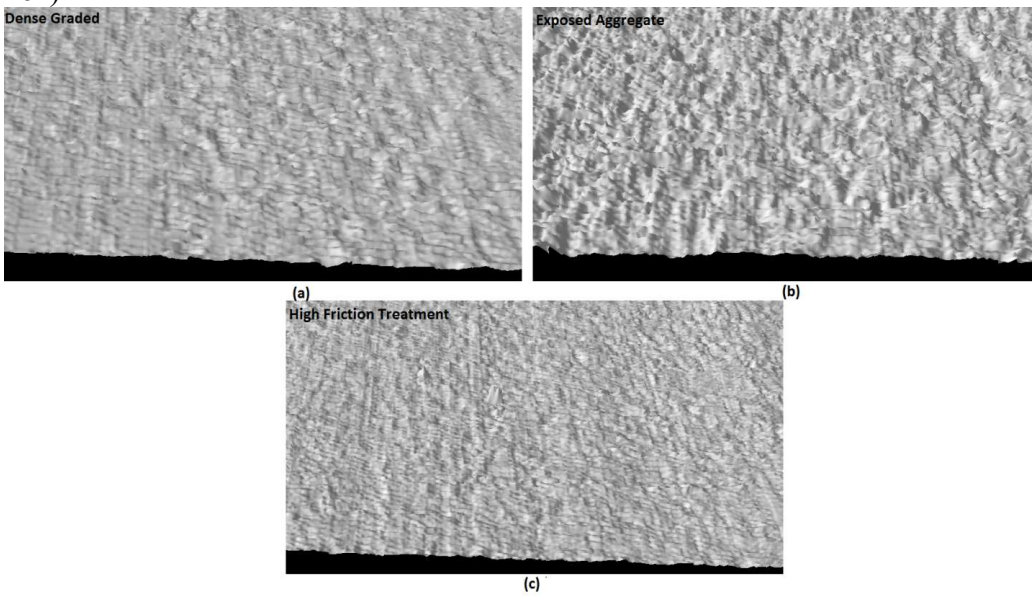

Figure 4.6. 3D rendering of flexible pavement test specimens from 3D Ultra

Correlation analyses are performed among the indicators with the following observations:

- Figure 4.7 shows there is no good correlation between *MPD* and other texture indicators with one exception of *SMTD*. In this case *MPD* is applied in model development to describe the amplitude property of surface texture.
- Figure 4.8 indicates a good correlation is observed between *RMS* and *SAR*, with an *R*-squared value of 0.9, and thus *SAR* is used to describe the hybrid property of surface texture.
- Figure 4.9 indicates no good agreements exist between *Skewness* and *Kurtosis* or *SBI*. Both of them should be kept to disclose surface texture properties.
- Figure 4.10 shows there is a poor correlation between *Kurtosis* and *SBI*.

Based on correlation analysis results, *MPD*, *Skewness*, *Kurtosis*, *TAR*, *SAR*, and *SBI* are capable of disclosing different aspects of surface texture properties, and are used for the development of pavement friction prediction model.

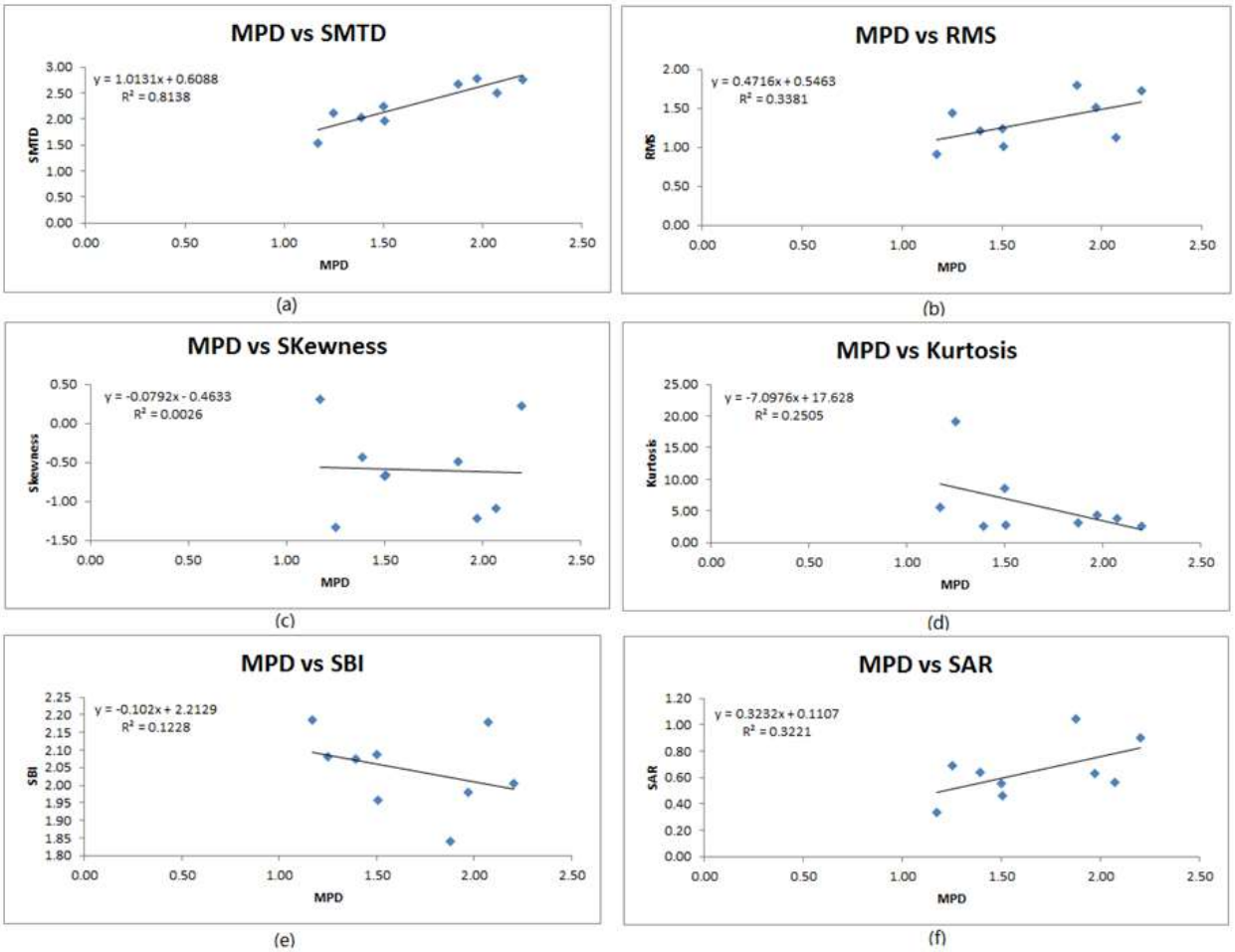

Figure 4.7. Correlation analysis results with MPD

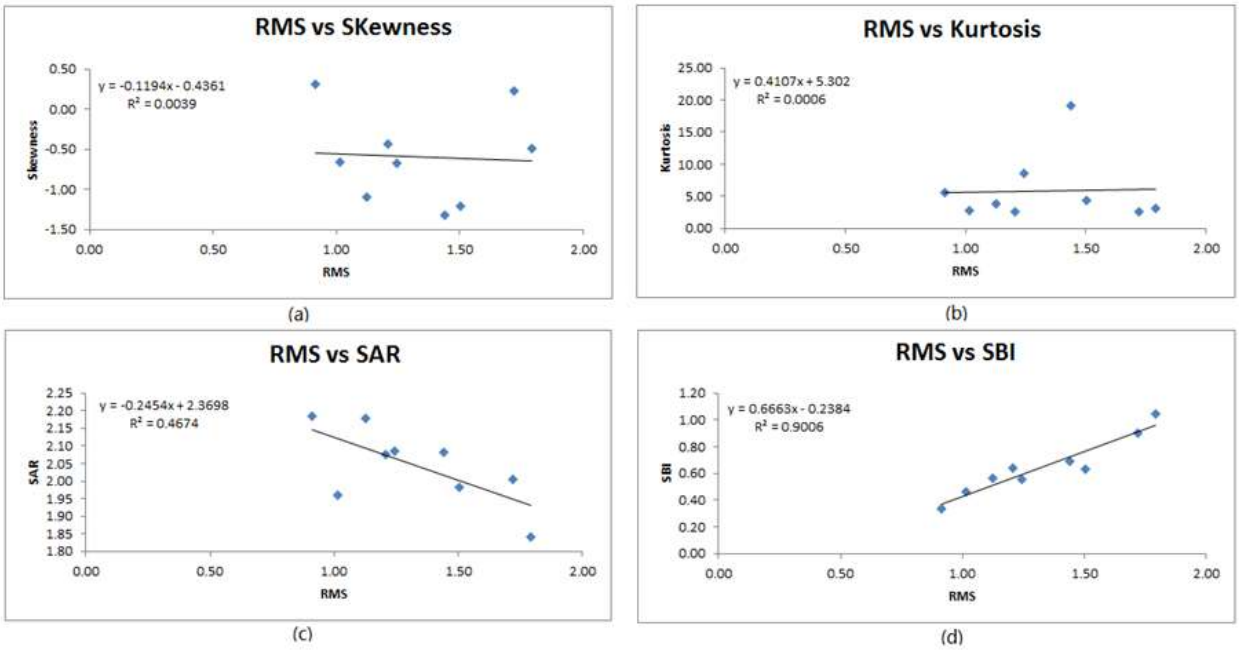

Figure 4.8. Correlations analysis results with RMS

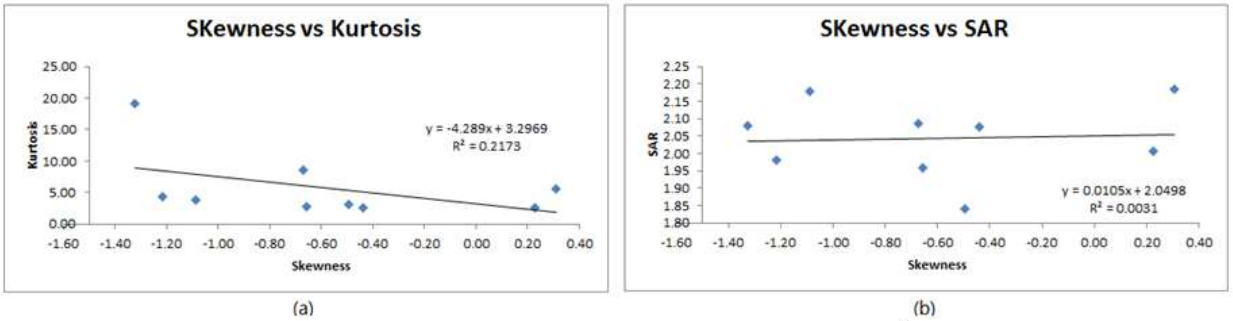

Figure 4.9. Correlation analysis results with skewness

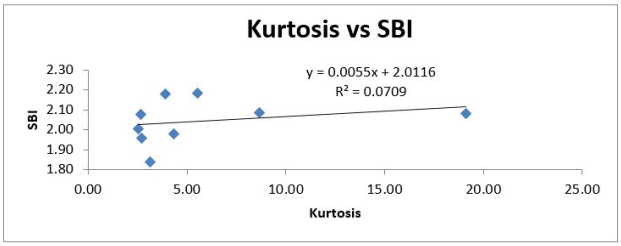

Figure 4.10. Correlation result between Kurtosis and SBI

Pavement Friction Model Development and Case Study

Route Description

To explore the relationships between the six surface texture indicators and pavement friction, one pavement section is chosen as the test bed in this study. AL-I 65 data collection starts at GPS coordinate of 32.387859, -86.322212, and ends at GPS coordinate of 32.390949, -86.321396, with a total length of approximately 393 m. The data collection site is the ramp from NB I-65 to EB SH152 (Northern Blvd.), as shown in Figure 4.11.

The route consists of two surface types: High Friction Surface Treatment (HFST) and the regular AC pavement surface type. HFST is located in the middle of the test section. The regular surface is located at the lead-in and lead-out segments.

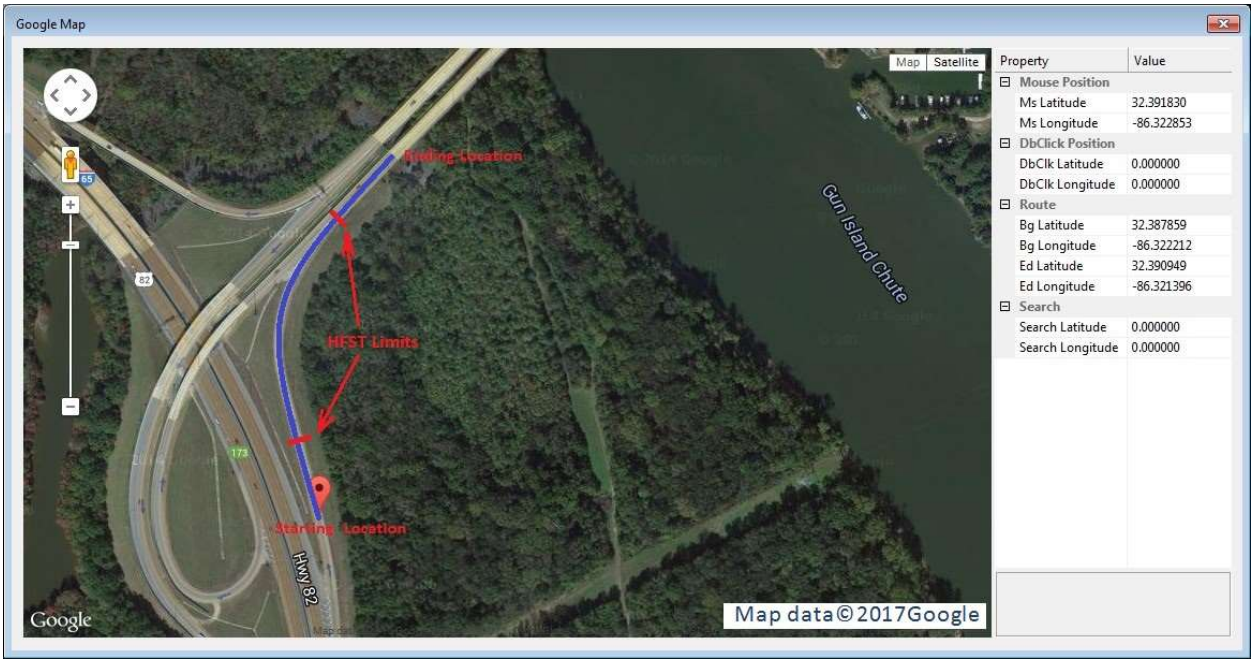

Figure 4.11. AL-I 65 HFST test site

Friction Field Measurement

In this study the friction data are acquired with the FHWA fixed-slip continuous friction tester, and 1mm 3D texture data are collected using DHDV with Pavesion3D Ultra. The test section is sampled into 84 segments, and each segment has a length of 4.57m (two 3D image long). The HFST segment starts from approximately 95 m and ends at approximately 301m, as marked in Figure 4.12.

To validate the reliability of the collected friction data, three repetitive measurements are conducted. Note that the three measurements show consistent results with the correlation coefficients of 0.95, 0.98, and 0.95, respectively. In this study the mean friction numbers (FNs) from the three measurements are used for model development and validation.

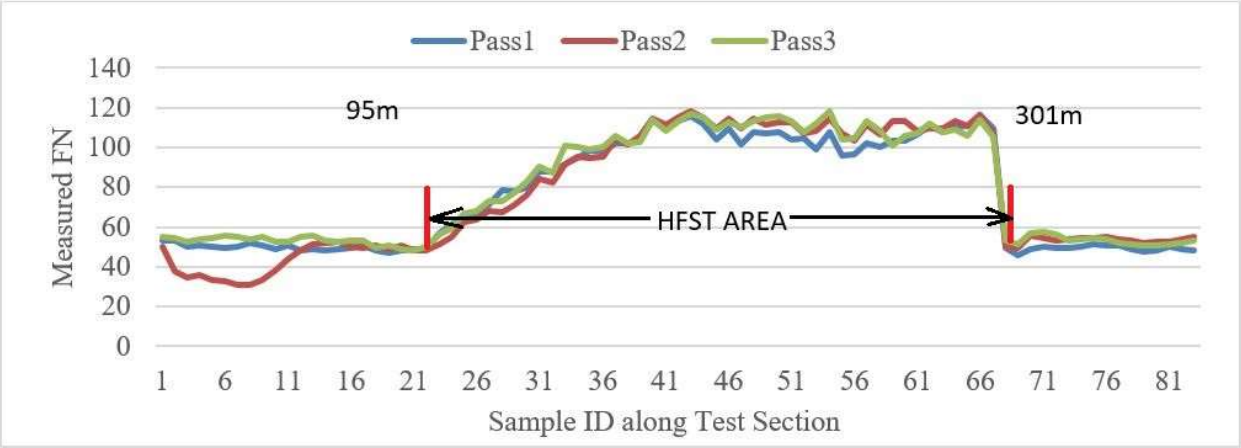

Figure 4.12. Friction measurement results on AL I 65 ramp

Pavement Friction Prediction

Model Development

As presented in Section 4, six texture indicators, namely *MPD*, *Skewness*, *Kurtosis*, *TAR*, *SAR*, and *SBI* are selected for pavement friction model development. Based on the multivariate regression analysis, pavement friction (FN_p) can be estimated with the six texture indicators, as mathematically described in Equation (4.10).

$$FN_p = 52.41MPD + 6.91Skewness - 1.15Kurtosis + 15.32TAR - 108.92SAR + 63.67SBI - 140.69 \quad (4.10)$$

Figure 4.13 shows the correlation results between the predicted and measured *FNs* based on the multivariate regression analysis, with an *R*-squared value of 0.868. The predicted and measured friction numbers are shown in Figure 4.14. In addition, the sensitivity analyses of the predicted *FNs* to the six texture indicators indicate that *Kurtosis* and *SAR* have no significant influences on the predicted *FNs* based on the p-values (e.g. p >0.05), as shown in Table 4.1. Accordingly pavement friction enables to be estimated with the four indicators: *MPD*, *Skewness*, *TAR*, and *SBI*.

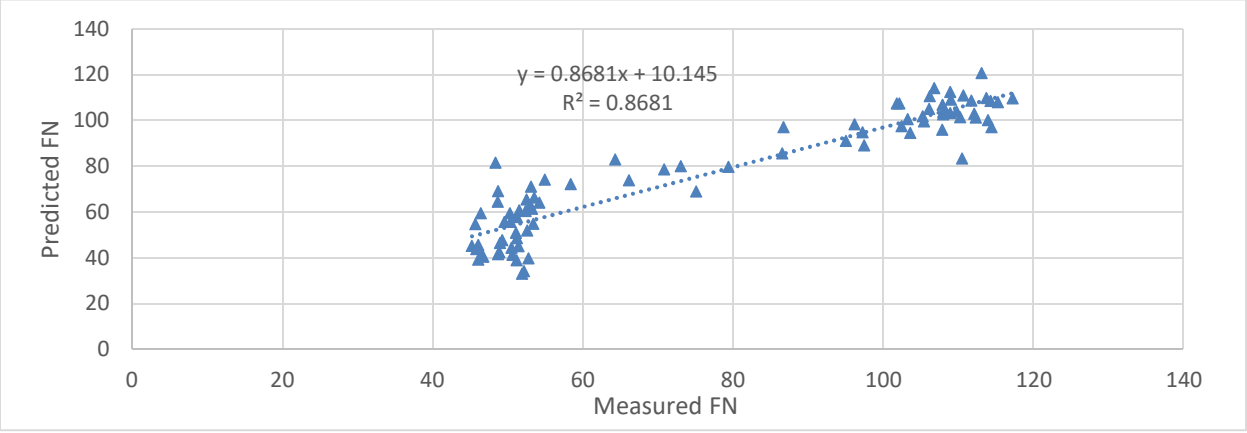

Figure 4.13. Correlation results between the predicted and measured FNs

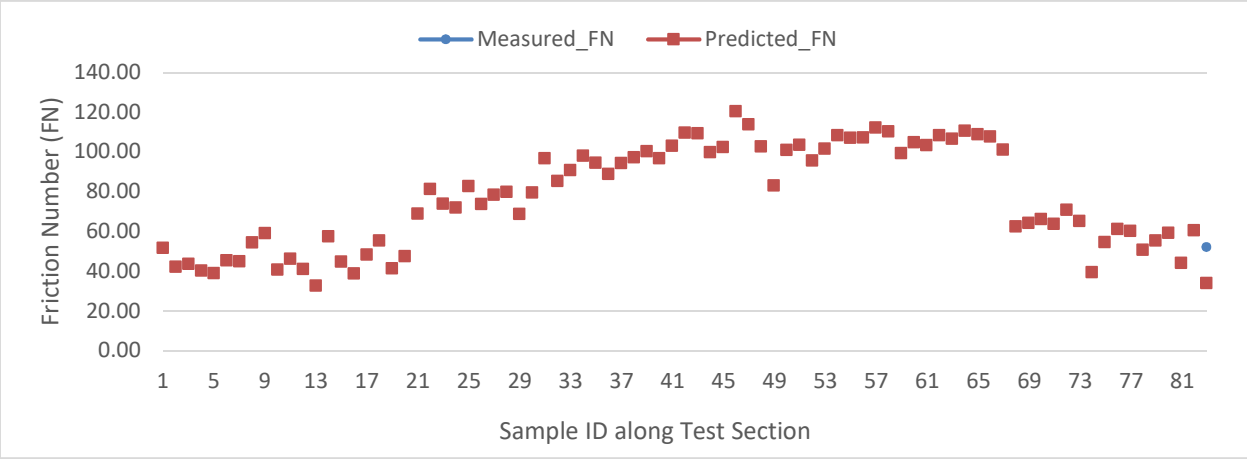

Figure 4.14. Comparison of the measured and predicted FNs from six texture indicators

Table 4.1. Multivariate regression results from the six texture indicators

Indicator	Coefficients	Standard Error	t Stat	p-value	Lower 95%	Upper 95%	Lower 95.0%	Upper 95.0%
Intercept	-140.69	29.02	-4.85	0.00	-198.48	-82.90	-198.48	-82.90
MPD	52.42	6.59	7.95	0.00	39.29	65.54	39.29	65.54
Skewness	6.91	1.77	3.90	0.00	3.38	10.45	3.38	10.45
TAR	15.32	5.47	2.80	0.01	4.42	26.23	4.42	26.23
SBI	63.67	5.02	12.69	0.00	53.68	73.67	53.68	73.67
Kurtosis	-1.15	3.50	-0.33	0.74	-8.13	5.82	-8.13	5.82
SAR	108.92	81.24	1.34	0.18	-52.89	270.72	-52.89	270.72

The multivariate regression analysis indicates the correlation coefficient between the predicted and measured *FNs* is around 0.86 when the four variables are used to estimate pavement friction, and the corresponding model coefficients are given in Table 4.2. Note that the p-value for each variable is less than 0.05, indicating the developed model is statistically significant for pavement friction prediction. The developed model can be mathematically described using Equation (4.11).

$$FN_p = 48.27\,MPD + 7.38Skewness + 12.34TAR + 59.42SBI - 105.58 \quad (4.11)$$

Table 4.2. Multivariate regression results from MPD, Skewness, TAR, and SBI

Indicator	Coefficients	Standard Error	t Stat	p-value	Lower 95%	Upper 95%	Lower 95.0%	Upper 95.0%
Intercept	-105.58	9.79	-10.78	0.00	-125.08	-86.09	-125.08	-86.09
MPD	48.27	5.96	8.09	0.00	36.39	60.14	36.39	60.14
Skewness	7.38	1.31	5.63	0.00	4.77	9.99	4.77	9.99
TAR	12.34	5.06	2.44	0.02	2.27	22.41	2.27	22.41
SBI	59.42	4.10	14.49	0.00	51.26	67.59	51.26	67.59

Model Verification and Improvement

In this model the effects of each independent variables (e.g. *MPD*) on dependent variables (e.g. *FN*) are assumed to be linear. If the effects of the independent variables on the dependent variables appear to be non-linear, this model may not be the appropriate fit for the data. In this study the residual plots is used to investigate the linear effects of independent variable on the dependent variable. The residual plot shows the residuals (the differences between the measured and predicted values) on the vertical axis and the independent variable on the horizontal axis. If the points in a residual plot are randomly distributed around the horizontal axis, a linear regression model may be appropriate for the data; otherwise, a non-linear model is more appropriate [48]. Figure 4.15 shows the residual plots of the four variables.

Note that the Figures 4.15b and 4.15d show a random dispersion around the horizontal axis, indicating the linear models can be applied on these two variables to predict pavement friction. Figures 4.15a and 4.15c show non-random patterns (U-shaped or inverted U-shaped) are observed for the *Skewness* and *TAR*, indicating the non-linear models should be used for the two variables. Based on Figure 4.16(a), a non-linear model should be developed to fit the FNs with the independent variable "MPD". After several trial-and-error, a three-order polynomial model is employed with the largest R-squared value. Similarly, exponential model is developed for the SBI to fit the measured FNs as shown in Figure 4.16b. Subsequently, data transformation is performed.

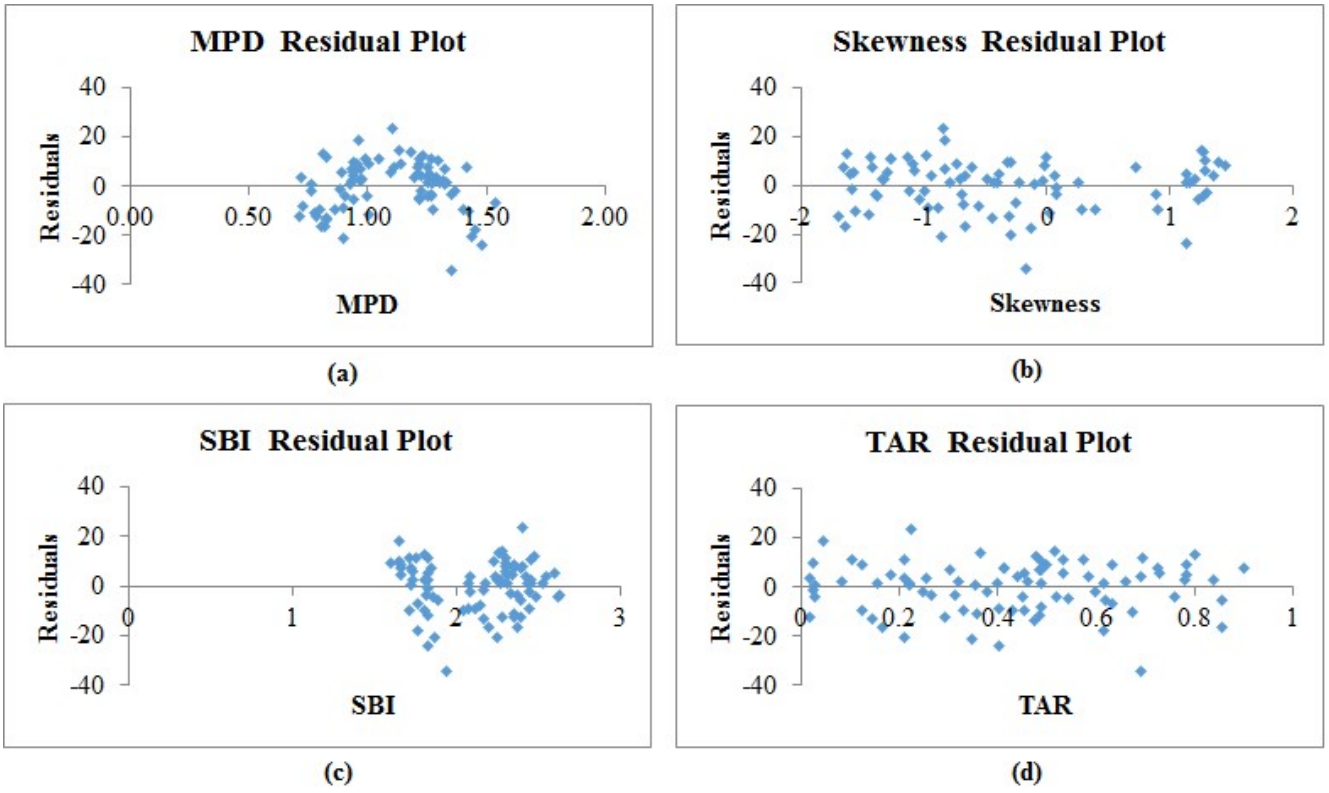

Figure 4.15. Residual plots of the four variables
a) MPD; b) Skewness; c) SBI; d) TAR

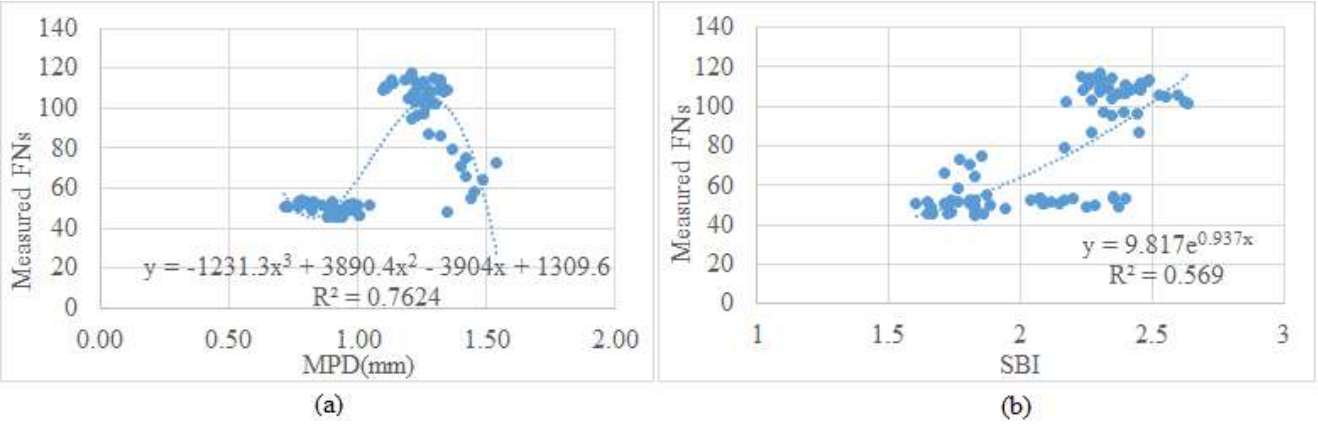

Figure 4.16. Non-linear models
a) MPD and b) SBI

In the subsequent multivariate analysis, the original MPD and SBI are replaced by the transformed MPD and SBI calculated from the developed models, and the multivariate regression analysis results are given in Table 4.3. Note that the p-values are approaching to the zero, indicating the newly developed model are statistically more significant for pavement friction prediction. As a result, a new model can be developed with the four variables: *MPD*, *Skewness*, *TAR*, and *SBI*, as mathematically described in Equation (4.12).

$$FN_p = -714.15\,MPD^3 + 2256.43MPD^2 - 2264.432MPD + 7.04Skewness + 13.43TAR + 5.89e^{0.94SBI} + 743.93 \quad (4.12)$$

Table 4.3. Multivariate regression results from Skewness, TAR, NEW_MPD and NEW_SBI

Indicator	Coefficients	Standard Error	t Stat	P-value	Lower 95%	Upper 95%	Lower 95.0%	Upper 95.0%
Intercept	-15.64	4.68	-3.34	0.00	-24.96	-6.32	-24.96	-6.32
Skewness	7.04	1.18	5.96	0.00	4.69	9.39	4.69	9.39
TAR	13.43	4.43	3.03	0.00	4.61	22.26	4.61	22.26
NEW_MPD	0.58	0.06	9.50	0.00	0.46	0.70	0.46	0.70
NEW_SBI	0.60	0.07	8.64	0.00	0.46	0.74	0.46	0.74

Correlation between the Predicted and Measured FNs

The measured *FNs* are correlated with the predicted *FNs* from the Equation 12, with an *R*-squared value of 0.895. Apparently there are three outliers among the test samples due to their large deviations from the fitting line, as illustrated in Figure 4.17a. After the influences of the outliers on the developed models are eliminated, a new linear model can be developed, with an *R*-squared value of 0.947, as shown in Figure 4.17b.

As a result, pavement friction can be estimated based on the four texture indicators: *MPD*, *Skewness*, *TAR*, and *SBI*. *MPD* and *Skewness* belong to the amplitude parameters representing

surface height distribution. *TAR* belongs to the spacing parameters, describing pavement surface texture pattern. *SBI* belongs to the functional parameters, disclosing surface bearing capacity and pavement frictional properties.

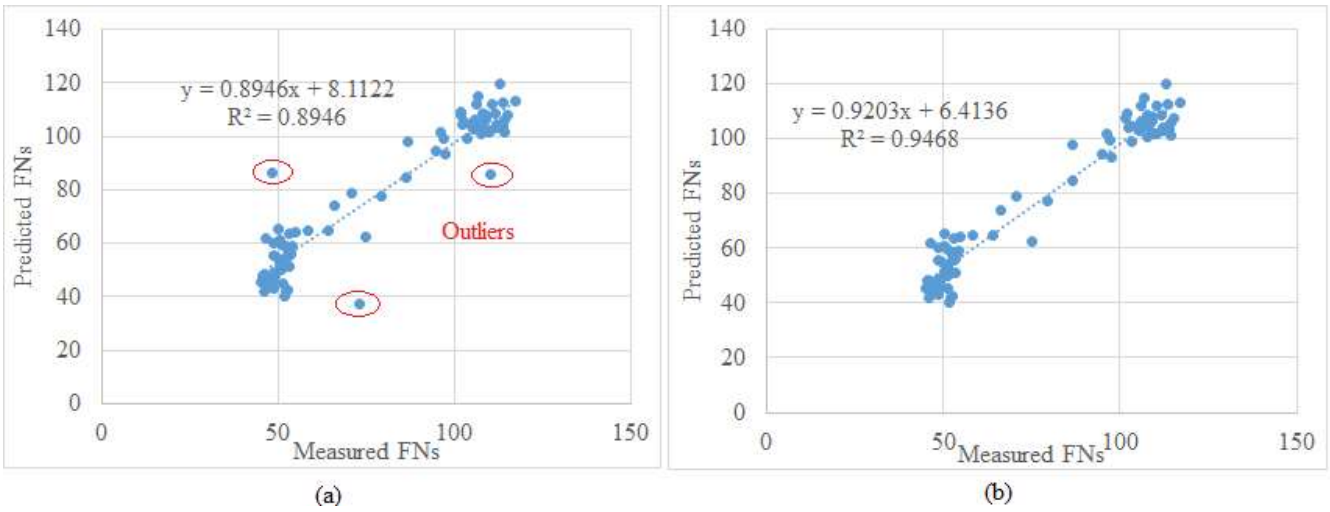

Figure 4.17. Correlation results between the predicted and measured FNs
a) with outliers; b) after outlier removal

5. EVALUATION OF PAVEMENT SURFACE HYDROPLANING

Introduction

Pavement hydroplaning occurs when water pressures build up in front of a moving tire resulting in an uplift force sufficient to separate the tire from the pavement. The loss of steering and traction force produced during hydroplaning may cause the vehicle to lose control, especially when a steering tire is involved [49]. Past studies indicated the event of hydroplaning is highly associated with several factors, including pavement texture, cross slope, longitudinal grade, pavement width, pavement types, pavement condition, tire characteristics, and rainfall intensity [50, 51].

Numerous field studies were dedicated to developing hydroplaning prediction models in the past decades [52]. The models can be grouped into two categories: empirical models and analytical models [53]. The empirical methods use experimental data and equations to predict hydroplaning, including Road Research Laboratory (RRL) equations to estimate water film depth (WFD) [54], National Aeronautics and Space Administration (NASA) models developed based on aircraft tire and airport pavement data (4), and Gallaway model to predict roadway hydroplaning [55]. The analytical methods attempt to mathematically model hydroplaning of the sheet flow and its interaction with a tire, including PAVDRN computer program developed by Pennsylvania State University [56], and the University of South Florida (USF) model based on Ong and Fwa's numerical prediction [57].

Pavement slope, also termed as flow path slope, consists of cross slope and longitudinal grade, which exerts a tremendous influence on hydroplaning prediction [58]. To maintain constant water film, hydroplaning simulation tests in past studies were conducted on pavements at tangent and flat terrain[59, 60]. For pavement segments with horizontal curve and severe down grade, a smaller uplift force of water can cause hydroplaning issues due to the reduced vertical wheel load caused by large slopes. However, past studies on hydroplaning prediction neglected the influences of pavement slope on vertical wheel loads of vehicles. The existing hydroplaning prediction models overestimate hydroplaning speed, and are particularly not suitable to analyze pavements with steep pavement slope.

Hydroplaning Prediction Models

Gallaway and USF Models

The Gallaway model is an empirical method developed by Gallaway et al. [55] for the US Department of Transportation. The method described in Equation (5.1)-(5.5) was adopted in the Texas Department of Transportation (TxDOT) *Hydraulic Design Manual* [55]. The flow path, an important factor on hydroplaning prediction model, can be defined in Figure 5.1 and calculated with Equation (5.1). The USF model is an analytical hydroplaning prediction model developed at the University of South Florida based on Ong and Fwa's comprehensive numerical prediction, shown in Equation (5.6). The USF model can be used to predict the hydroplaning speeds for different light vehicles that employ tires compatible with the locked-wheel tester tires [57].

$$S_f = (S_l^2 + S_c^2)^{1/2} \quad (5.1)$$

$$L_f = W_p \times (S_f / S_c) \quad (5.2)$$

$$WFD = 0.01485\left[(MTD^{0.11} \times L_f^{0.43} \times I^{0.59})/(S_c^{0.42})\right] - MTD \quad (5.3)$$

$$A = \text{Max. of}\begin{cases} \left(\frac{12.639}{WFD^{0.06}}\right) + 3.50 \\ \left[\left(\frac{22.351}{WFD^{0.06}}\right) - 4.97\right] \times MTD^{0.14} \end{cases} \quad (5.4)$$

$$v_p = 0.9143 \times SD^{0.04} \times P_t^{0.3} \times (TD + 0.794)^{0.06} \times A \quad (5.5)$$

$$v_p = W^{0.2} \times P_t^{0.5} \times \left[\left(\frac{0.82}{WFD^{0.06}}\right) + 0.49\right] \quad (5.6)$$

Where, WFD: Water film depth (mm); MTD: Mean texture depth (mm) calculated from the macro texture data; v_p: Hydroplaning speed (km/h); L_f: Pavement flow path length (m); S_c: Cross slope (m/m); S_l: Longitudinal grade (m/m); W_p: Pavement width (m); I: Rainfall intensity (mm/hr); P_t: Inflation pressure (Kpa); SD: Spin down ratio; TD: Tire tread depth (mm); W: Wheel load (N).

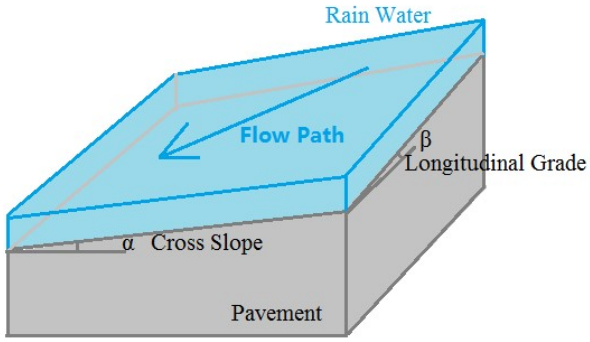

Figure 5.1. Schematic diagram of cross slope, longitudinal grade, and flow path

Effects of Pavement Slope on Vertical Wheel Load

Typically cross slope or longitudinal grade would reduce the vertical wheel load of vehicles on pavement surface [61]. Hydroplaning occurs when the vertical wheel load is equivalent to the uplift force by water (Equation (5.7)), and the steering and traction force would be lost during hydroplaning.

Figure 5.2 (a) shows the pavement section with a large longitudinal grade. When the vehicle travels on this pavement segment, the vehicle gravity center would be partitioned into two components of forces: one (wheel load) is perpendicular with the travelling surface, and the other one (traction force) is parallel with pavement surface. The wheel load would decrease with the increase of longitudinal grade (Equation (5.8)), and the reduced wheel load would increase the hydroplaning risk.

Figure 5.2 (b) shows the pavement section with horizontal curves or large cross slope. Similarly, the vehicle gravity center is partitioned into two components of forces when the vehicle travels on the horizontal curve. One component of force is the wheel load, and the other one is the centripetal force shown in Figure 5.2 (b). The wheel load on horizontal curve would decrease with the increase of super-elevation (Equation (5.9)). Finally the wheel load can be calculated with flow path slope by combining the cross slope and longitudinal grade, as given in Equation (5.10).

$$F_{Up} = W \tag{5.7}$$

$$W_L = G \times cos(\beta) \tag{5.8}$$

$$W_C = G \times cos(\alpha) \tag{5.9}$$

$$W = G \times cos(\rho) \tag{5.10}$$

Where: F_{Up} -- Minimum uplift force causing hydroplaning (N); W -- Wheel load (N); W_L -- Wheel load in longitudinal section (N); W_C -- Wheel load in cross section (N); G -- Gravity of vehicle (N); β -- Angle of longitudinal grade (degree); α-- Angle of cross slope (degree); ρ -- Angle of flow path slope (degree).

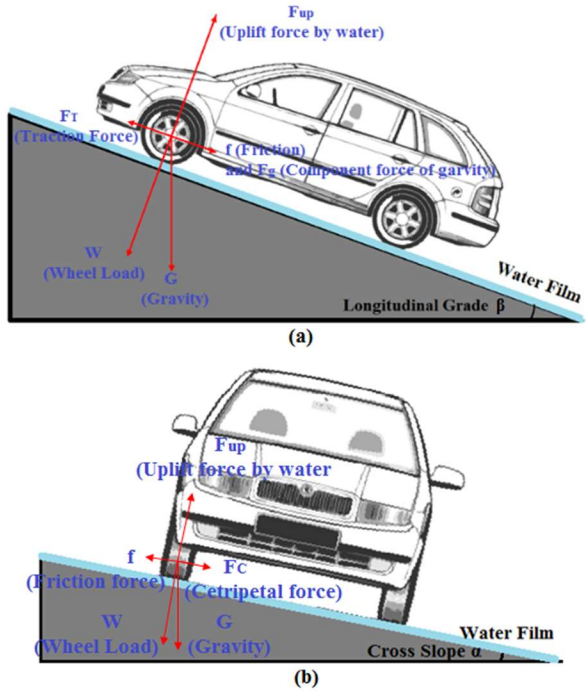

Figure 5.2. Vehicle travelling on pavements with (a) longitudinal grade; (b) horizontal curve

Improved Hydroplaning Speed Prediction Models

In the current models, the influences of flow path slope on vertical wheel load are not taken into account in hydroplaning prediction models. Therefore this study aims at improving the existing

Gallaway and USF models by considering the effects of flow path slope on wheel loads, as shown in Equations (5.11) and (5.12).

$$v_p = 0.9143 \times SD^{0.04} \times (P_t \times cos\rho)^{0.3} \times (TD + 0.794)^{0.06} \times A \quad (5.11)$$

$$v_p = (W \times cos\rho)^{0.2} \times (P_t \times cos\rho)^{0.5} \times (0.82/WFD^{0.06} + 0.49) \quad (5.12)$$

Where: W -- Wheel load (N); WFD -- Water film depth (mm); P_t -- Inflation pressure (Kpa); SD -- Spin down ratio; TD -- Tire tread depth (mm); A -- Maximum value of Equation (4); ρ -- Angle of flow path slope (degree).

Sensitivity Analysis of the Improved Models

To explore the sensitivity of cross slope and longitudinal grade on hydroplaning speed, the cross slope and longitudinal grade change by ± 25%, ± 50%, and ± 75% individually while the other variables are maintained constant values. The constant values of each factor is assumed to be the average values of that factor measured for test site, as provided as follows:

- Cross slope: $S_c = 1.53\%$
- Rainfall intensity: $I = 148.4\ mm/hr$
- Mean texture depth: $\mathrm{MTD} = 1.2$ mm
- Longitudinal grade: $S_l = 1.32\%$

The results of sensitivity analysis from the improved Gallaway and USF models to cross slope and longitudinal grade are given in Figure 3. It can be seen that the resulting change in hydroplaning speed, "V_P", is apparent along the increase of cross slope and longitudinal grade. In the two improved models, the hydroplaning speed is affected by both the vertical load and the flow path length. Typically the increase in cross slope or longitudinal grade would diminish the vertical wheel load. The increase in cross slope would shorten the flow path length, while the increase in longitudinal grades would extend the flow path length. Both the decrease in vertical load and the increase in flow path length would reduce the hydroplaning speed.

Accordingly the hydroplaning speed should decrease with the increase of longitudinal slope, and may either increase or decrease with the increase of cross slope depending on effects of vertical load and flow paths. Figure 5.3 shows that hydroplaning speed goes up with the increase of the cross slope, indicating the effect of flow path length on hydroplaning speed is greater than that of wheel load. It is shown that hydroplaning speed is more sensitive to the cross slope than longitudinal grade in the two improved models.

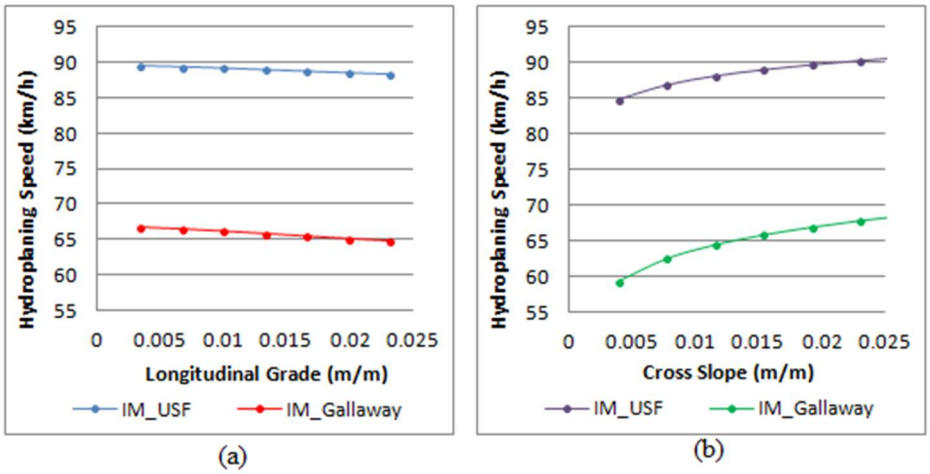

Figure 5.3. Sensitivity of improved hydroplaning models
(a) longitudinal grade; (b) cross slope

Data Preparation

Estimated Mean Texture Depth (EMTD)

The methodologies for texture measurements can be grouped into two categories: static and high-speed methods. The static test methods include Sand Patch Method [26], Circular Track Meter [24], and Outflow Meter [62], and their measurements are conducted on the marked or specified small areas. The traditional high-speed test techniques are characterized with the laser based data acquisition systems [63] with a spot laser resulting in a single line of measurement along the longitudinal direction of pavement. The measurements are continuously conducted on test sections, which can be regarded as an efficient tool for network level pavement survey.

The widely used texture indicators include the Mean Profile Depth (MPD) and Mean Texture Depth (MTD) [25, 26]. In this study the MTD methodology is applied since the estimation of water film depth is dependent on the MTD in the hydroplaning models. However, as the manual process to obtain MTD through the Sand Patch Method is a standard, time-consuming, and somewhat not reliable enough [47], the 3D pavement surface captured with the 3D Ultra technology is therefore used as an alternative to be used as input to calculate area texture simulating the Sand Patch Method. The alternative substantially improves data collection efficiency and reliability of computing surface texture. As a volumetric method, the Estimated MTD (EMTD) is therefore introduced in the research by simulating the Sand Patch Method with 1mm 3D laser imaging data of the entire lane, as shown in Equation 5.13 [47]. EMTD and MTD are assumed to be equivalent in the presented research.

$$EMTD = (1/k) \times \sum_{i=1}^{K} \frac{\iint_0^D [F_0 - F(x,y)]dxdy}{D} = (1/k) \times \sum_{i=1}^{K} \frac{\sum_{x=1}^{x=N} \sum_{y=1}^{y=M} [F_0 - F(x,y)]}{D} \quad (5.13)$$

Where: $F(x,y)$ – The pixel depth at point (x, y); D – The integral or gridded area containing of M×N pixels; F_0 – The maximum peak in each area D; K – The number of grids within the test sample.

Cross Slope Calibration

A properly designed and constructed cross slope is important for safe travelling since inadequate cross slopes may result in low efficiency in drainage and steep cross slopes may lead to vehicle maneuvering difficulties. Therefore the accurate measurement of cross slope is important for hydroplaning speed prediction. In this study, 1mm 3D pavement data and IMU data are combined together to reproduce the cross slope of pavements.

IMU mounted on the vehicle can measure three Euler angles, which are termed as roll (Euler angle about x-axis), pitch (Euler angle about y-axis) and yaw (Euler angle about z-axis) respectively. The roll angle is to represent pavement cross slope, and pitch angle is traditionally used to represent pavement longitudinal grade based on the assumption that the vehicle floor is parallel with pavement surface during travelling. However, in real world the vehicle floor is not parallel with pavement surface during travelling, which can be caused by: 1) uneven gravity distribution of the vehicle; 2) vibration of the vehicle during travelling; 3) pavement surface geometry and condition.

This study attempts to measure the vehicle's body roll angle in X coordinate (angle γ) using the collected 3D laser imaging data. Two sensors mounted on the rear of the DHDV are capable of covering the entire lane. The "true" cross slope of pavements can be approximately determined with two parameters: the tilt of the vehicle floor and the slope of pavement surface captured by 3D cameras [47]. As Figure 5.4 shows, the IMU system measures the angle θ of the vehicle relative to a level datum. γ is the vehicle vibration angle in X coordinate which can be calculated in Equation (5.14). The "true" cross slope can be obtained by Equation (5.15). However, in real world the angle θ and γ are very small, so the cross slope can be directly computed as the difference in slope of θ and slope of γ (Equation (5.16)) [64].

$$\gamma = \text{act}\tan\left(\frac{y_2 - y_1}{L}\right) \quad (5.14)$$

$$\alpha = \tan(\theta + \gamma) \quad (5.15)$$

$$\alpha = \tan(\theta) + \tan(\gamma) \quad (5.16)$$

Where: α – Angle of cross slope (degree); γ – The body roll angle of vehicle (degree); θ – IMU roll angle (degree); L – The distance between left and right laser (m); y_1 – The vertical distance from left sensor to the pavement surface (m); y_2 – The vertical distance from right sensor to the pavement surface (m).

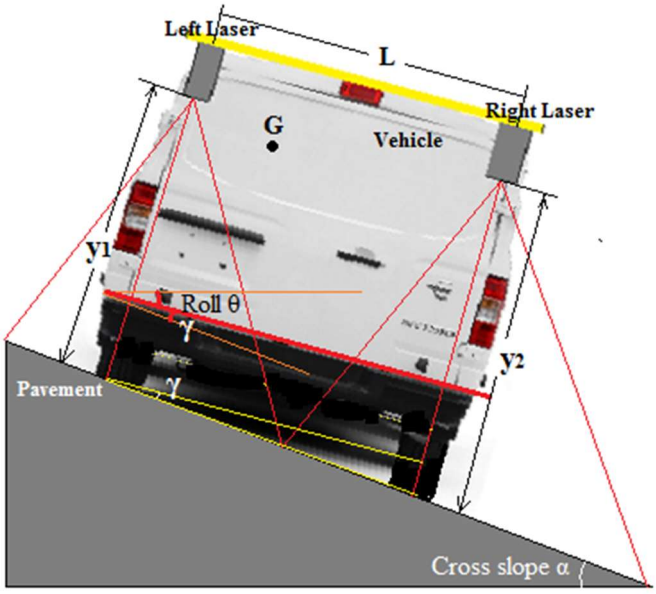

Figure 5.4. Cross slope calibration based on IMU and 1mm 3D data

Software Interface for Automated Hydroplaning Prediction

A software program named Automated Hydroplaning Prediction Program (AHPP) is developed in this study to implement data processing and analysis. Figure 5.5 shows the main interface of AHPP. Once users import the IMU and 3D image data into AHPP, the two types of data (1mm 3D laser imaging data and IMU data) can be automatically matched by Distance Measurement Instrument (DMI) pulses, and the calibrated cross slope can be produced by the integration of IMU data and 3D data. In AHPP, users can manually assign the local rainfall intensity and pavement types. The AHPP outputs include EMTD, WFD, calibrated cross slope, longitudinal grade, and predicted hydroplaning speeds from various models.

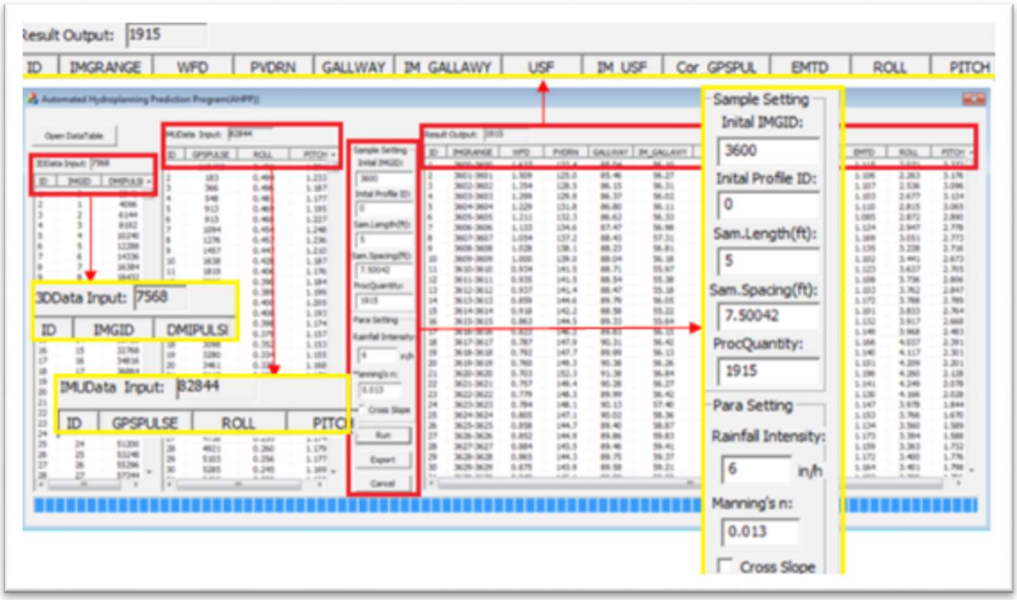

Figure 5.5. Software interface for automated hydroplaning prediction

Case Study

Testing Site

A flexible pavement section located in Spavinaw, Oklahoma is chosen as the test section, which starts from the location (Latitude: 36.329175, Longitude: -95.081696), and ends with the location (Latitude: 36.351066, Longitude: -95.062796), with a length of 4.35 km. The pavement of the test lane is in excellent condition and has a width of 3.65m. On this test section there are five horizontal curves.

Selection of Sample Size

The 3D laser imaging data collected with the 3D Ultra DHDV is stored on computer hard disk in the form of raw data files with the size of 4096 pixel wide by 2048 pixel long. The raw data files are used as basic input data sets, or samples, and subsequently data processing and analysis are conducted on each individual sample. In this study one raw image is considered as a sample (2.28m long) and the entire pavement section consists of 1915 samples.

Local Rainfall Intensity

The local rainfall intensity at the test site is obtained from National Oceanic and Atmospheric Administration's (NOAA) National Water Service database [65]. Table 5.1 shows the precipitation in Spavinaw Station Oklahoma from NOAA database. The two-year return period storm with duration of five minutes is used in Gallaway and USF models for rainfall intensity acquisition. Based on NOAA database, the rainfall intensity of 148.4mm/hour is used for the test site.

Table 5.1. Precipitation in Spavinaw station

Duration (in mm)	Recurrence - 1 year	Recurrence - 2 year	Recurrence - 5 year	Recurrence - 10 year
5 min	10.87	12.37	14.91	17.04
10 min	15.93	18.11	21.82	24.97
15 min	19.41	22.09	26.67	30.48
30 min	28.70	32.77	39.62	45.47

Cross Slope and Longitudinal Grade

Both longitudinal grade and cross slope are the key factors to form flow path slope. As Figure 5.6(a) shows, the maximum longitudinal grade is 12.03%, and the standard deviation is 2.48. Due to the vibration of the surveying vehicle, there is some noise in the raw cross slope captured by IMU roll angle. Based on the 3D laser imaging data, the vehicle body roll angle can be measured, and then the raw cross slope is calibrated. Figure 5.6(b) shows the raw cross slope and calibrated cross slopes. Comparing the raw cross slope data and calibrated cross slope, the majority of the noise is eliminated from the raw data through the calibration. The cross slope presents negative values at left turn curves and positive values at right turn curves. In this test site, curves #1, #4, and #5 belong to left turn curve, while curves #2 and #3 belong to right turn curve. The statistical results of the calibrated cross slopes on test site are given as follows: (1) the

average cross slope on the straight road segments is 1.94%; (2) the average cross slope of curve #1, #2, #3, #4, and #5 are -2.06%, 4.96%, 5.80%, -3.81%, and -5.01%, respectively.

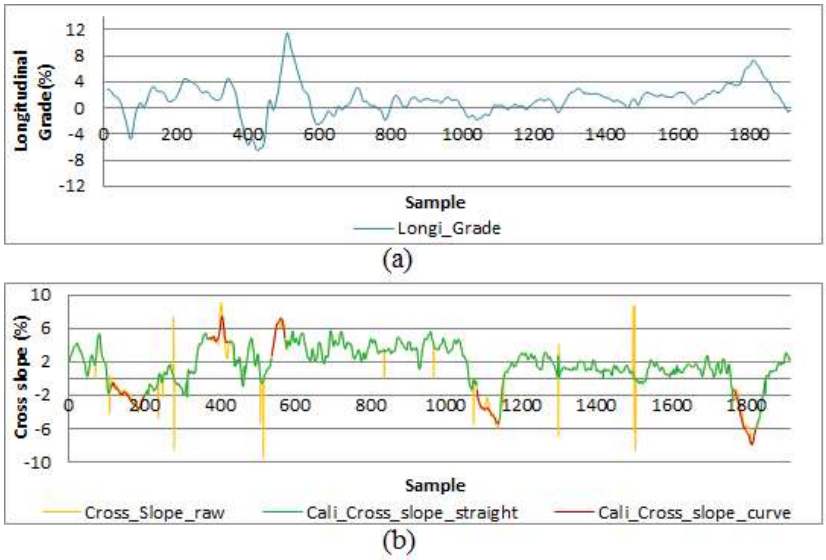

Figure 5.6. Pavement geometry of the testing site
(a) Longitudinal grade; (b) Cross slope.

EMTDs and WFDs

Figure 5.7(a) shows the corresponding WFD along the test section, with an average value of 1.73mm and the maximum value of 8.52 mm, and Figure 5.7(b) shows the EMTDs at the test section, with an average value of 1.20 mm. The WFD is calculated with Gallaway WFD model based on pavement texture depth, flow path slope, and local rainfall intensity as inputs.

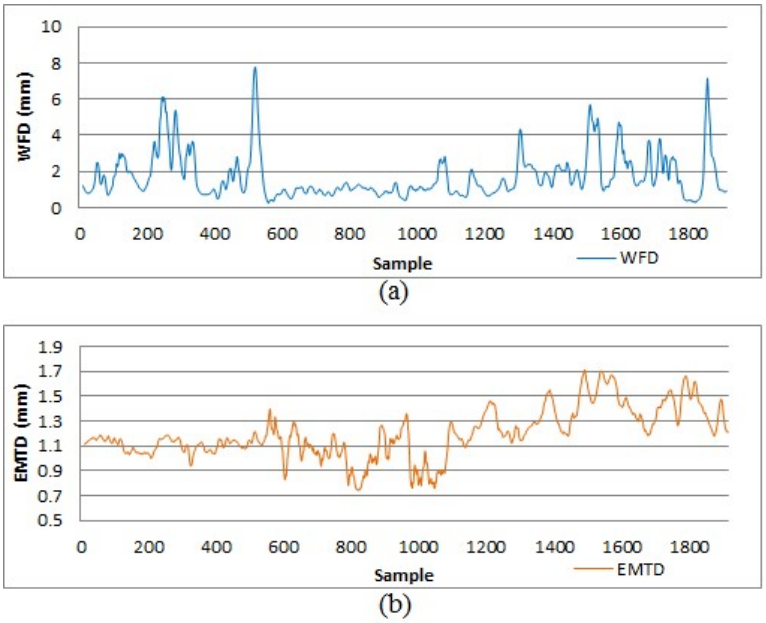

Figure 5.7. WFDs and EMTDs of test site
(a) WFDs; (b) EMTDS.

Hydroplaning Speed Estimation

15 samples of the calculated WFD, EMTD and IMU data for hydroplaning speed prediction are given in Table 5.2. Gallaway model, USF model, the improved Gallaway model, and the improved USF model are utilized to predict hydroplaning speed, respectively, as shown in Figure 10(a). Results indicate the predicted hydroplaning speeds from original Gallaway and USF model are approximately 140km/h and 165km/h, respectively, which are around 50km/h higher than those predicted from the improved Gallaway model (96km/h) and improved USF model (91km/h). The results also show as expected that the hydroplaning speeds at curves of the five horizontal curves in Figure 5.8(a) are lower than that on the straight road sections.

Table 5.2. Sample 3D and IMU data for hydroplaning speed calculation

Sample ID	WFD (mm)	EMTD (mm)	Cross Slope (%)	Longitudinal Grade (%)
1	1.64	1.12	2.07	3.27
2	1.51	1.11	2.26	3.18
3	1.35	1.11	2.54	3.10
4	1.30	1.10	2.68	3.12
5	1.23	1.11	2.82	3.07
6	1.21	1.09	2.87	2.89
7	1.13	1.12	2.95	2.78
8	1.05	1.17	3.05	2.77
9	1.03	1.14	3.23	2.72
10	1.00	1.10	3.44	2.67
11	0.93	1.12	3.64	2.71
12	0.94	1.11	3.74	2.81
13	0.94	1.10	3.76	2.85
14	0.86	1.17	3.79	2.79
15	0.92	1.10	3.83	2.76

Potential Hydroplaning Segment Detection

Identification of locations with hydroplaning potential is based on the comparison of estimated hydroplaning speed with posted speed of the road section [47]. At the test site, speed limits are 80km/h on straight sections and 56km/h on road curves. The average hydroplaning speeds calculated with the four models are used to detect potential hydroplaning segments, shown in Figure 5.8(a). Since the predicted hydroplaning speeds at the five curves are higher than posted speed limit, there is a low hydroplaning risk at the five curves for vehicles operating at speed limit. However, for several segments of the test site, the predicted hydroplaning speeds are lower than the posted speed limit. Therefore, these segments can be identified as potential segments for increased hydroplaning risk, as marked with red line in Figure 5.8(b). To minimize traffic crashes caused by hydroplaning, highway agencies can post a reduced speed sign at these locations, or take other remedial actions, such as installing High-Friction Surface Treatment (HFST) [66].

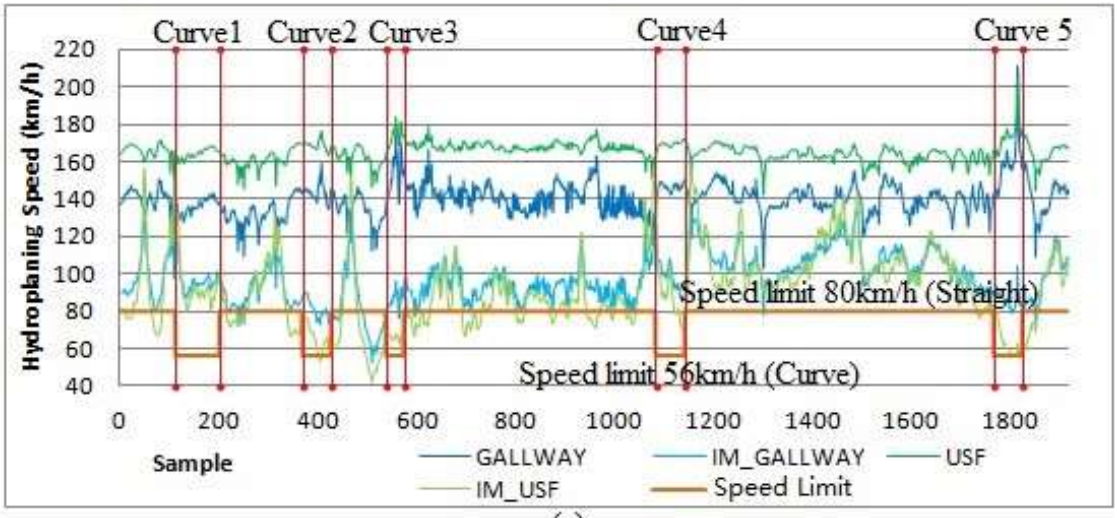

(a)

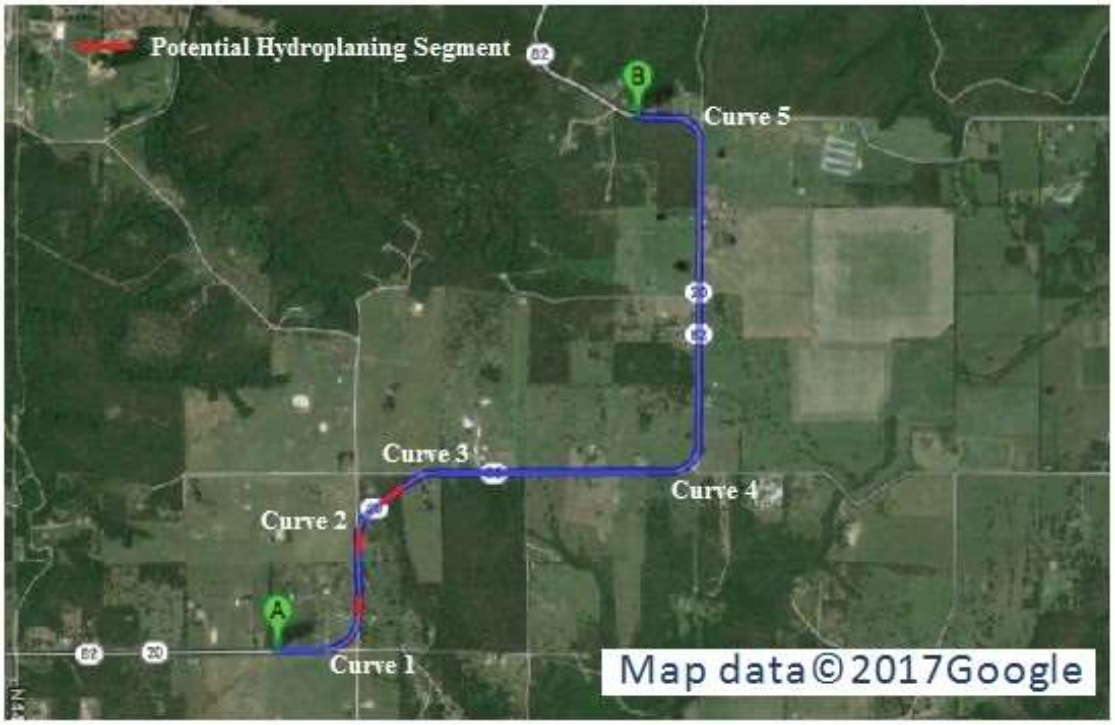

(b)

Figure 5.8. Detection of potential hydroplaning risk
(a) hydroplaning speed; (b) increased hydroplaning potential segments.

6. SUMMARY

The 3D Ultra laser imaging technology has the capability to collect pavement surface texture data at full-lane coverage at 1 mm resolution in all three dimensions at speed up to 60MPH. This single-pass and complete lane coverage platform provides an ideal solution to evaluate pavement surface characteristics for safety analysis and many different data collection needs without interrupting traffic. Furthermore, it will saved cost by eliminating the need for maintenance of traffic.

In this study, the 3D Ultra laser imaging technology with necessary software tools are utilized for data collection and subsequent surface characterization and safety evaluation and analysis. First, the 1mm 3D data for 21 HFST sites in 11 states with a total of 41 sections are collected for each traffic lane at the posted highway speeds. Pavement rutting and macro-texture data are calculated from collected 1mm 3D data sets, while pavement friction data are collected using FHWA's fixed-slip continuous friction tester. The measured surface characteristics on the HFST sites and untreated existing pavements are compared and paired t-tests are performed to determine the effectiveness of the HFST sites in improving surface characteristics. It is evident that the HFST surfaces have statistically significant higher friction numbers and surface macro-texture MPD values than those on the adjacent pavements without HFST. There exist several exceptions to such trend, 2 sections for friction data and 5 sections for MPD data. Multivariate analyses are conducted to investigate the impacts of five independent variables: precipitation, average temperature, HFST installation age, aggregate type, and AADT, on HFST friction performance. Average temperature and HFST installation age are identified to have significantly impact on friction performance of HFST (FN_{HFST}) and the ratio of friction on HFST to that on non-HFST (FN Ratio). Based on the trend between FN Ratio and installation age, in general the benefit of HFST in friction effectiveness is lost after approximate 60 months (5 years) of service. HFST sites using calcined bauxite aggregates exhibit higher friction performance than those using flints. The regressional friction prediction models are therefore developed for HFST, which can be used to predict the service life of HFST installation and aid decision making within a highway agency. However, it should be noted that the models don't consider the pavement conditions before HFST application and HFST construction quality variations as the dependent variables due to the unavailability of data. In addition, detailed traffic data for ramps and each lane of sites with multiple lanes are not available and have to be estimated during the model development.

Surface texture and friction are two primary characteristics for pavement safety evaluation. Understanding their relationship is critical to reduce potential traffic crashes especially at wet conditions. However, the currently used texture indicators, such as Mean Profile Depth (*MPD*), and Mean Texture Depth (*MTD*), are calculated restricted on either a small portion on pavement surface or single line of profile measurement, and thus only reveal partial aspects of texture property. With 1mm 3D laser texture data, eight surface texture indicators are examined for their applications on pavement friction prediction. The eight surface texture indicators are grouped into four categories: amplitude parameters (including MPD, SMTD, RMS, Skewness, and Kurtosis), spacing parameters (TAR), hybrid parameters (SAR), and functional parameters (SBI). To avoid using two highly correlated texture indicators in the friction prediction model, correlation analyses are conducted and found that 1) SMTD are highly correlated with MPD; 2)

RMS is highly correlated with SAR. As a result, six texture indicators, including MPD, Skewness, Kurtosis, TAR, SAR, and SBI, are adopted for the development of pavement friction prediction model using multivariate regression analysis. The developed model can be used to predict pavement friction based on various texture indicators, and may be beneficial in the continuous measurement and evaluation of pavement safety for the project- and network- level pavement surveys.

The third application of using 1mm 3D Ultra data sets is to predict and evaluate pavement surface hydroplaning risk. Considering the effects of flow path slope on vertical wheel load perpendicular to pavement surface and the resulting hydroplaning speed, the Gallaway and USF models are modified for improvements in this study. The sensitivity analysis shows that the hydroplaning speed is more sensitive to cross slope than longitudinal grade in the improved models. A 3D based volumetric measuring method is used to calculate the estimated MTD based on the full-lane 1mm 3D data. Subsequently, IMU data and 3D data are combined to model vehicle movements on cross slopes. Local rainfall intensity is obtained from NOAA precipitation database. By considering effects of cross slope and longitudinal grade on wheel load and flow path length, it is found that hydroplaning speed decreases with the increase of the longitudinal grade, but increases with the increase of the cross slope. The improved models predict lower hydroplaning speed than that from the original Gallaway and USF models. An important future work is to use a combined slope based on longitudinal grade and cross slope to demonstrate the validity and effectiveness of the improved models.

This study with field pavement applications has shown that the 1mm 3D Ultra which represent a form of 3D Laser imaging technology is promising in real-time pavement surface characterization and evaluation for both pavement and safety management at network and project level surveys. It is anticipated that more data collection with more testing sites are to be performed to validate the new emerging 3D laser imaging technology as a single-pass and complete lane-coverage platform for multiple safety and pavement evaluation purposes. In addition, the long-term monitoring of the HFTS sites in multiple states is highly recommended due to the need to determine multi-year performance of the HFTS applications in terms of region, pavement condition, materials used, geometric properties, and other factors. The recommended long-term study would provide much needed data for both design and construction of HFTS for its widespread adoption.

REFERENCES

[1] Brimley B. and Carlson P. Using High Friction Surface Treatments to Improve Safety at Horizontal Curves. Texas Transportation Institute. http://d2dtl5nnlpfr0r.cloudfront.net/tti.tamu.edu/documents/TTI-2012-8.pdf, 2012 (accessed 15.06.25).

[2] The Trans Tec Group, INC. Welcome to High Friction Roads. http://www.highfrictionroads.com, 2015 (accessed 15.07.25).

[3] Bledsoe J. Missouri Demonstration Project: The Use of High-Friction Surface Treatments on Missouri Highways. FHWA, U.S. Department of Transportation. http://plan4operations.dot.gov/hfl/summary/pdf_2/Missouri%20High%20Friction%20Report%20draft%20Final.pdf, 2015 (accessed 15.06.30).

[4] Moravec M. High Friction Surface Treatments at High-Crash Horizontal Curves. Arizona Pavements/Materials Conference, Phoenix, AZ. http://www.intrans.iastate.edu/events/midcon2013/documents/presentation-submissions/3-C_61_08142013.pdf, 2013 (accessed 15.06.30).

[5] South Dakota Department of Transportation (SDDOT). Accelerated Innovation Deployment (AID) Demonstration Project: High Friction Surface Treatment. http://www.fhwa.dot.gov/accelerating/grants/pdfs/SD_2014_AID_Grant.pdf, 2015 (accessed 15.06.11).

[6] Bischoff D. Investigative Study of the Italgrip ™ System. WI-04-08. Wisconsin Department of Transportation, Madison, WI. http://wisdotresearch.wi.gov/wp-content/uploads/wi-04-08italgrip.pdf, 2008 (accessed 15.06.20).

[7] Izeppi E., Flintsch G. and McGhee K. Field Performance of High Friction Surfaces. Publication FHWA/VTRC 10-CR6. FHWA, U.S. Department of Transportation. http://www.virginiadot.org/vtrc/main/online_reports/pdf/10-cr6.pdf, 2010 (accessed 15.06.15).

[8] Waters J. High Friction Surfacing Failure Mechanisms. 3rd International Surface Friction Conference, Safer Road Surfaces – Saving Lives, Gold Coast, Australia. 2011.

[9] Wang Kelvin C. P. Elements of Automated Survey of Pavements and a 3D Methodology. J. mod. transp., Vol. 19, pp: 51-57, 2011.

[10] AASTHO. *Quantifying cracks in asphalt pavement surfaces from collected images utilizing automated methods*. AASHTO Designation PP67-10. American Association of State Highway and Transportation Officials. Washington, D.C., 2013.

[11] AASTHO. 2013. Standard Practice for Determining Pavement Deformation Parameters and Cross Slope from Collected Transverse Profiles. AASHTO Designation: PP69-10. American Association of State Highway and Transportation Officials. Washington, D.C., 2013.

[12] Hall, J. W., Smith, K. L., Titus-Glover, L., Wambold, J. C., Yager, T. J., and Rado, Z. Guide for Pavement Friction. Final Report for NCHRP Project 01-43. National Cooperative

Highway Research Program (NCHRP), Transportation Research Board (TRB), Washington D.C., 2009.

[13] Ahammed M.A. and Tighe S.L. Concrete Pavement Surface Textures and Multivariables Frictional Performance Analysis: a North American Case Study. *Can. J. Civil. Eng.*, Vol 35 727-738, 2008.

[14] Ergun M., Iyinam S., and Iyinam A.F. Prediction of Road Surface Friction Coefficient Using Only Macro- and Microtexture Measurements. *J. Transp. Eng.*, Vol. 131, pp: 311-319, 2005.

[15] Flintsch G.W. et al. The Little Book of Tire Pavement Friction. Pavement Surface Properties Consortium. https://secure.hosting.vt.edu/www.apps.vtti.vt.edu/1-pagers/CSTI_Flintsch/The%20Little%20Book%20of%20Tire%20Pavement%20Friction.pdf, 2012 (accessed 15.05.01).

[16] Henry, J. J. NCHRP Synthesis 291: Evaluation of Pavement Friction Characteristics. TRB, National Research Council, Washington, D.C., 2000.

[17] Ahammed M.A. and Tighe S.L.. Effect of Short-term and Long-term Weather on Pavement Surface Friction. *Int. J. N.a. Res. Tech.*, Vol. 3, pp: 295-302, 2010.

[18] Luo Y. Effect of Pavement Temperature on Frictional Properties of Hot-Mix-Asphalt Pavement Surfaces at the Virginia Smart Road. M.S. Thesis, Virginia Polytechnic Institute and State University, Blacksburg, Va. 2003.

[19] Fuents L. G. Investigation of the Factors Influencing Skid Resistance and the International Friction Index. PhD. Thesis, University of South Florida, Tampa, FL. 2009.

[20] American Society for Testing and Materials (ASTM). ASTM E 867: Standard Terminology Relating to Vehicle-Pavement Systems, *ASTM Standard Practice E 867 Book of ASTM Standards*, Volume 04.03 Philadelphia, P A, 2011.

[21] International Standards Organization (ISO). Characterization of Pavement Texture using Surface Profiles – Part 1: Determination of Mean Profile Depth, Acoustics, *ISO Standard 13473, International Standards Organization*, Geneva, Switzerland, 1998.

[22] PIARC World Road Association. Report of the Committee on Surface Characteristics. In *Proceeding of XVIII World Road Congress*, Brussels, Belgium, pp: 13–19, 1987.

[23] Sandburg, U. Influence of Road Surface Texture on Traffic Characteristics Related to Environment, Economy, and Safety: A State-of-the-Art Study Regarding Measures and Measuring Methods, *VTI Report 53A-1997*, Swedish National Road Administration, Borlange, Sweden, 1998.

[24] American Society for Testing and Materials (ASTM). ASTM E 2157: Standard Test Method for Measuring Pavement Macro texture Properties Using the Circular Track Meter, *ASTM Standard Practice E 2157 Book of ASTM Standards*, Volume 04.03 Philadelphia, P A, 2011.

[25] American Society for Testing and Materials (ASTM). ASTM E 1845: Calculating Pavement Macro texture Profile Depth, *ASTM Standard Practice E 1845 Book of ASTM Standards*, Volume 04.03 Philadelphia, P A, 2011.

[26] American Society for Testing and Materials (ASTM). ASTM E 965: Standard Test Method for Measuring Pavement Macro texture Depth Using a Volumetric Technique, *ASTM Standard Practice E 965 Book of ASTM Standards*, Volume 04.03 Philadelphia, P A, 2011.

[27] McGhee, K. K., & Flintsch, G. W. High-speed Texture Measurement of Pavements. Virginia Transportation Research Council, Charlottesville, VA, 2003.

[28] Prowell, B., & Hanson, D. Evaluation of Circular Texture Meter for Measuring Surface Texture of Pavements. *Transportation Research Record: Journal of the Transportation Research Board*, No. 1929, pp: 88-96, 2005.

[29] Alvarez, L., & Morel, J. M. Formalization and Computational Aspects of Image Analysis. *Acta numerica*, Vol. 3, pp: 1-59, 1994.

[30] Gendy, A. E., & Shalaby, A. Mean Profile Depth of Pavement Surface Macrotexture Using Photometric Stereo Techniques. *Journal of Transportation Engineering*, Vol. 133 No. 7, pp: 433-440, 2007.

[31] Kokkalis, A. and Panagouli, O. Fractal Evaluation of Pavement Skid Resistance Variations. I: *Surface Wetting. Chaos, Solitons & Fractals*, pp: 1875-1890, 1998.

[32] American Society for Testing and Materials (ASTM). ASTM E 274: Standard Test Method for Skid Resistance of Paved Surfaces Using a Full-Scale Tire, *ASTM Standard Practice E 274 Book of ASTM Standards*, Volume 04.03 Philadelphia, P A, 2011.

[33] American Society for Testing and Materials (ASTM). ASTM E 303: Standard Test Method for Measuring Surface Frictional Properties Using a British Pendulum Tester, *ASTM Standard Practice E 303 Book of ASTM Standards*, Volume 04.03 Philadelphia, P A, 2011.

[34] Janoo, V.C., and Horhonen C. Performance Testing of Hot-Mix Asphalt Aggregates, Special Report, pp: 99-20, 1999.

[35] Kuennen, T. Creating Friction Where Rubber Meets the Road, *Better Roads*, Vol. 73 No. 10, 2003.

[36] Leu, M.C., Henry, J.J. Prediction of skid resistance as a function of speed from pavement texture measurements. *Transportation Research Record,* No. 666, pp: 7-13, 1978.

[37] Yager, T. J., and Buhlmann, F. Macrotexture and Drainage Measurements on a Variety of Concrete and Asphalt Surfaces, *Pavement Surface Characteristics and Materials*, *ASTM STP 763*, pp: 16-30, 1982.

[38] Rado, Z. Analysis of Texture Models*, PTI Report No. 9510*, Pennsylvania Transportation Institute (PTI), Penn State University, State College, Pennsylvania, 1994.

[39] Fwa, T. F, Choo, Y. S., and Liu, Y., (2003). Effect of Aggregate Spacing on Skid Resistance of Asphalt Pavement, *Journal of Transportation Engineering*, Vol 129 No. 4, pp: 420-426, 2003.

[40] Olek, J., Weiss, W. J., and Garcia-Villarreal, R. Relating Surface Texture of Rigid Pavement with Noise and Skid Resistance, Purdue University, West Lafayette, Indiana, *Report No. SQDH-2004-1* (Final Report HL 2004-1), 2004.

[41] Do, M.T., Marsac, P., Delanne, Y. Prediction of Tire/wet Road Friction from Road Surface Microtexture, and Tire Rubber Properties. In: *5th International Symposium on Pavement Surface Characteristics*, Toronto, 2004.

[42] Ergun, M., Iyinam, S., & Iyinam, A. F. (2005). Prediction of Road Surface Friction Coefficient Using only Macro- and Micro texture Measurement, *Journal of transportation engineering*, Vol. 131 No. 4, pp: 311-319, 2005.

[43] Kebrle, J., Walker, R. Texture measurement and friction estimation using laser data acquisition and neural networks. In: *Proceedings of the 9th WSEAS International Conference on Mathematical and Computational Methods in Science and Engineering*, Trinidad and Tobago, 2007.

[44] Rezaei, A., Masad, E., Chowdhury, A., & Harris, P. Predicting Asphalt Mixture Skid Resistance by Aggregate Characteristics and Gradation, *Transportation Research Record: Journal of the Transportation Research Board*, No. 2014, pp: 24-33, 2009.

[45] American National Standards Institute. Surface texture: surface roughness, waviness and lay. American Society of Mechanical Engineers. 1986.

[46] Stout, K. J.; Sullivan, P.J.; Dong, W.P.; Mainsah, E., Luo, N.; Mathia, T.; and Zahyouani, H. The development of methods for the characterization of roughness in three dimensions. Commission of the European Communities, 1993.

[47] Luo, Wenting, Wang, Kelvin C. P., Li, Lin 2014 Surface Drainage Evaluation for Rigid Pavements Using IMU and 1 mm 3D Texture Data, Transportation Research Record: *Journal of the Transportation Research Board*, Washington, D.C, Pavement Management 2014, Volume 3, pp 121–128, 2014.

[48] Tsai, C. L., Cai, Z., & Wu, X. (1998). The examination of residual plots. *Statistica Sinica*, Vol. 8, pp: 445-465, 1998.

[49] Kumar, S.Santosh, Anupam, Kumar, and FWA, T.F. Analyzing effect of tire groove patterns on hydroplaning speed, *Journal of the Eastern Asia Society for Transportation Studies*, Vol. 8. 2009

[50] Khedr, Safwan A. and Breakah, Tamer M. Rutting parameters for asphalt concrete for different aggregate structures, *International Journal of Pavement Engineering*, Volume 12, Issue 1, pp 13-23, 2011.

[51] M.ISH, Rohit Goyal, Design and Analysis of Interceptor Drains—Effect of Parameters, *ISH Journal of Hydraulic Engineering*, Volume 9, Issue 1, pp 61-71, 2003.

[52] Horne, W.B., and R.C. Dreher. Phenomena of Pneumatic Tire Hydroplaning, NASA TN D-2-56, NASA Langley Research center, NASA, Hampton, VA, 1963

[53] Chesterton, John, Nancekivell, Noel, and Tunnicliffe, Noel, The use of the Gallaway Formula for Aquaplaning Evaluation in New Zealand, *Transit New Zealand and New Zealand Institute of Highway Technology (NZIHT) 8thAnnual Conference*, 2006.

[54] Russam, K. and Ross, N.F. The Depth of Rain Water on Road Surfaces. Road Research Laboratory, *Ministry of Transport Report* No. LR 236, pp25, 1968.

[55] Gallaway, B. M., et al. Pavement and Geometric Design Criteria for Minimizing Hydroplaning," Federal Highway Administration, Report No. FHWA-RD-79-31, 1979.

[56] Huebner. R.S., et al. PAVDRN Computer Model for Predicting Water Film Thickness and Potential or Hydroplaning on New and Reconditioned Pavements, *Transport Research Record* 1599 pp. 128-131, 1996.

[57] Gunaratne, M., Lu, Q., Yang, J., Hydroplaning on Multi Lane Facilities, Report for Florida Department of Transportation, Report No. BDK84 977-14, 2012.

[58] Zhang, Zhongjie , Abu-Farsakh, Murad Y. and Tao, Mingjiang, Evaluation of trench backfills at highway cross-drains, *International Journal of Pavement Engineering*, Volume 6, Issue 2, pp77-87, 2005.

[59] Gallaway, B. M., and Rose, Gerry, The Effects of Rainfall Intensity, Pavement Cross Slope, Surface Texture, and Drainage Length on Pavement Water Depths, Texas Transportation Institute, Research Report No. 138-5, 1971.

[60] Ong, G.P. and Fwa, T.F., Wet-pavement hydroplaning risk and skid-resistance: Modeling, *ASCE Journal of Transportation Engineering,* Vol. 133, No. 10, 2007.

[61] Shafabakhsh G.A., Kashi E., "Effect of Aircraft Wheel Load and Configuration on Runway Damages", *Period. Polytech. Civil Eng.,* Vol. 59, No. 1, pp. 85-94, 2015.

[62] ASTM, Measuring Pavement Texture Drainage Using an Outflow. ASTM Standard Practice E 2380 *Book of ASTM Standards, Volume 04.03* Philadelphia, P A, 2006.

[63] ASTM, Measuring Surface Frictional Properties Using the British Pendulum Tester, ASTM Standard Practice E 303 *Book of ASTM Standards, Volume 04.03* Philadelphia, P A, 2006.

[64] Mekemson et al., Method and Apparatus for Pavement Cross-slope Measurement, Patent Application Publication, Pub. No.: US 2002/0013644 A1, 2002.

[65] NOAA's National Water Service, Hydrometeorological Design Studies Center, "Precipitation Frequency Data Server (PFDS)": http://dipper.nws.noaa.gov/hdsc/pfds/, Accessed on July, 2014.

[66] Shah, Yogesh U. , Jain, S.S. , and Parida, Manoranjan, Evaluation of prioritization methods for effective pavement maintenance of urban roads, *International Journal of Pavement Engineering*, Volume 15, Issue 3, pp 238-250, 2014.

For More Information:

Safety Analysis Opportunities Using Pavement Surface Characterization Based on 3D Laser Imaging, visit: http://safety.fhwa.dot.gov/

U.S. Department of Transportation
Federal Highway Administration

July 2017
FHWA-SA-17-046